NAVAL POSTGRADUATE SCHOOL
Monterey, California

THESIS

A WATER TUNNEL INVESTIGATION OF A SMALL SCALE ROTOR OPERATING IN THE VORTEX RING STATE

by

Charles B. Rumsey Jr.

June 2003

Thesis Advisor: E. Roberts Wood
Co-Advisor: Steven R. Baker

Approved for public release; distribution is unlimited

THIS PAGE INTENTIONALLY LEFT BLANK

REPORT DOCUMENTATION PAGE

Form Approved OMB No. 0704-0188

1. AGENCY USE ONLY ***(Leave blank)***	**2. REPORT DATE** June 2003	**3. REPORT TYPE AND DATES COVERED** Master's Thesis

4. TITLE AND SUBTITLE A Water Tunnel Investigation of a Small Scale Rotor Operating in the Vortex Ring State

5. FUNDING NUMBERS

6. AUTHOR (S) Charles B Rumsey, Jr.

7. PERFORMING ORGANIZATION NAME(S) AND ADDRESS(ES)
Naval Postgraduate School
Monterey, CA 93943-5000

8. PERFORMING ORGANIZATION REPORT NUMBER

9. SPONSORING / MONITORING AGENCY NAME(S) AND ADDRESS(ES)
N/A

10. SPONSORING/MONITORING AGENCY REPORT NUMBER

11. SUPPLEMENTARY NOTES The views expressed in this thesis are those of the author and do not reflect the official policy or position of the U.S. Department of Defense or the U.S. Government.

12a. DISTRIBUTION / AVAILABILITY STATEMENT
Approved for public release; distribution is unlimited

12b. DISTRIBUTION CODE

13. ABSTRACT ***(maximum 200 words)***

Motivation to expand the understanding of a helicopter rotor descending into the vortex ring state (VRS) stems from the aircraft mishaps that have plagued the helicopter community. The V-22 has become the most recent victim of encounters with VRS.

The onset of VRS is associated with the collapse of the helical vortex wake in the plane of the rotor. The resulting wake disturbances develop an irregular and aperiodic flow. Rotor blade interaction with the disturbed vortices causes large variations in the blade spanwise aerodynamic load distribution. Harmonic analysis of the loading indicates that higher harmonic content becomes prevalent in this state.

The dynamic flow similarities achieved in a water tunnel are used to explore flow visualization and conduct vibration analysis of a rotor system operating in the VRS. A scaled rotor system was operated in the NPS Aeronautical Engineering Department's water tunnel. Sensors were used to gather thrust and vibration power spectrum data when operating in VRS. Experimental results correlate with full scale flight data and show a significant increase in the vibration levels of the even multiples of the blade passage frequency. The relative strength of these higher harmonics can be used as an indicator of impending VRS encounters.

14. SUBJECT TERMS Vortex Ring State, Power Settling, VRS, Water Tunnel, Vibration Analysis of VRS, Harmonics of VRS	**15. NUMBER OF PAGES** 77
	16. PRICE CODE

17. SECURITY CLASSIFICATION OF REPORT	**18. SECURITY CLASSIFICATION OF THIS PAGE**	**19. SECURITY CLASSIFICATION OF ABSTRACT**	**20. LIMITATION OF ABSTRACT**
Unclassified	Unclassified	Unclassified	UL

NSN 7540-01-280-5500 **Standard Form 298 (Rev. 2-89) Prescribed by ANSI Std. 239-18**

THIS PAGE INTENTIONALLY LEFT BLANK

Approved for public release; distribution is unlimited

A WATER TUNNEL INVESTIGATION OF A SMALL SCALE ROTOR OPERATING IN THE VORTEX RING STATE

Charles B. Rumsey Jr.
Major, United States Marine Corps
B.S., Virginia Polytechnic Institute and State University, 1987

Submitted in partial fulfillment of the
requirements for the degree of

MASTER OF SCIENCE IN APPLIED PHYSICS

from the

NAVAL POSTGRADUATE SCHOOL
June 2003

Author: Charles B. Rumsey Jr.

Approved by: E. Roberts Wood
Thesis Advisor

Steven R. Baker
Co-Advisor

William B. Maier, II
Chairman, Department of Physics

THIS PAGE INTENTIONALLY LEFT BLANK

ABSTRACT

Motivation to expand the understanding of a helicopter rotor descending into the vortex ring state (VRS) stems from the aircraft mishaps that have plagued the helicopter community. The V-22 has become the most recent victim of encounters with VRS.

The onset of VRS is associated with the collapse of the helical vortex wake in the plane of the rotor. The resulting wake disturbances develop an irregular and aperiodic flow. Rotor blade interaction with the disturbed vortices causes large variations in the blade spanwise aerodynamic load distribution. Harmonic analysis of the loading indicates that higher harmonic content becomes prevalent in this state.

The dynamic flow similarities achieved in a water tunnel are used to explore flow visualization and conduct vibration analysis of a rotor system operating in the VRS. A scaled rotor system was operated in the NPS Aeronautical Engineering Department’s water tunnel. Sensors were used to gather thrust and vibration power spectrum data when operating in VRS. Experimental results correlate with full scale flight data and show a significant increase in the vibration levels of the even multiples of the blade passage frequency. The relative strength of these higher harmonics can be used as an indicator of impending VRS encounters.

THIS PAGE INTENTIONALLY LEFT BLANK

TABLE OF CONTENTS

LIST OF FIGURES

LIST OF TABLES

THIS PAGE INTENTIONALLY LEFT BLANK

ACKNOWLEDGEMENTS

I would like to thank the Naval Postgraduate School Department of Aeronautics and Astronautics for the generous support in funding and resources in conducting this thesis. Great appreciation goes to all the professors in the Department of Physics who gave me the education to conduct this research. I thank my thesis advisor, Dr. E. Roberts Wood for his insightful guidance as well as persistent enthusiasm through the completion of this undertaking. His graceful mentoring provided for a most enjoyable learning experience. I would also like to thank Dr. Steven R. Baker for his exceptional assistance in matters of fluid dynamics and participating as a greatly appreciated co-advisor. I would be negligent if I did not express tremendous gratitude for the assistance provided by Jerry Lentz for devoting unimaginable effort over numerous days. He provided foundational support for the entire project. I especially would like to thank my wife, Karissa, and my daughters, Alissa and Robin, for supporting and tolerating me during this extremely time consuming endeavor.

THIS PAGE INTENTIONALLY LEFT BLANK

I. INTRODUCTION

A. MOTIVATION FOR RESEARCH

The need for increased understanding of the aerodynamic effects of the vortex ring state (VRS) has become an issue of great importance, since the mishap involving the tilt rotor V-22 Osprey and the primary causal factor determined as asymmetrical vortex ring state. In fact, thirty-four documented helicopter incidents involving encounters with the vortex ring state (VRS) occurred between 1982 and 2003. [Varnes, 1999]

To expand the understanding of this flow phenomenon, the development of a hydrodynamic facility to explore the flow field of a rotor system operating in the vortex ring state was undertaken. An experiment was conducted in the Naval Postgraduate School Aeronautical Engineering Department water tunnel, taking advantage of flow similarity factors, which permitted reduced operating velocity. The limited research conducted using a water tunnel also motivated studying this flow phenomena in a new medium. This thesis demonstrates that VRS boundary limits can be mapped and relevant vibration analysis can be performed on rotor systems operating in a water tunnel.

B. HELICOPTER ROTOR FLOW STATES

A rotor in vertical flight is typically described as being in one of three flow states. These are: (1) propeller working state; (2) vortex ring state; and (3) windmill brake state.

1. Propeller Working State

The propeller working state is terminology used to indicate vertical climb conditions, Figure 1. Airflow is

through the rotor in the opposite direction of thrust. During the propeller working state the trailing tip vortices are downstream of the path of each subsequent passing rotor blade. The limiting condition of the propeller working state is the hover. [Stewart, 1951]

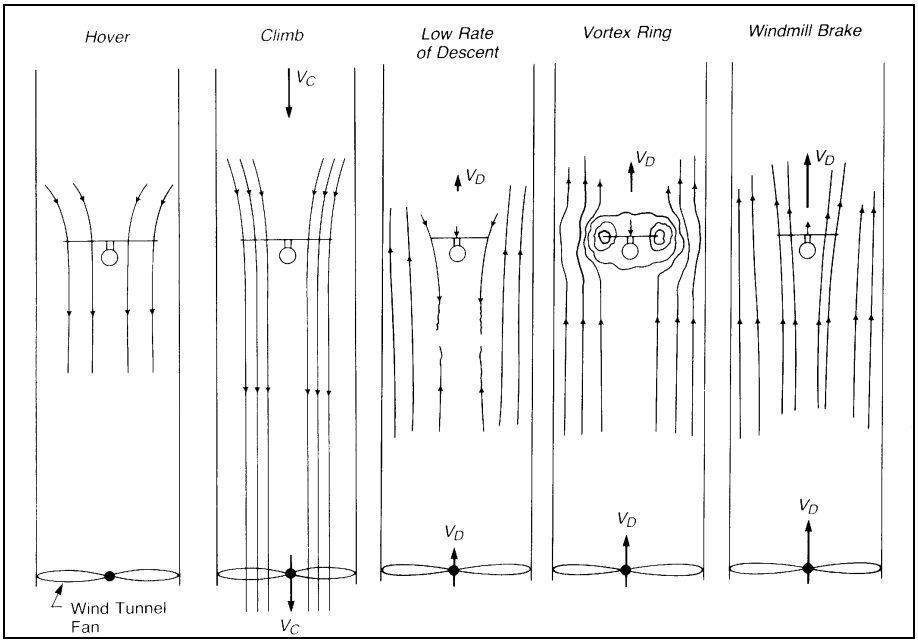

Figure 1. Helicopter Flow States. [From: Prouty, 1986]

2. Vortex Ring State

The blade tip vortices, which normally cause minor losses in rotor efficiency, can be drastically enlarged when the aircraft begins to descend into its own downwash, Figure 1. Blades begin to recirculate the downwash quickly back above the rotor disk, only to be recirculated back down again. The airflow through the rotor plane does not have a regular slipstream, but flow is thrust out radially and recirculated. The rotor blades can eventually begin to stall as the angle of attack is increased due to the upward

airflow. Prior to blade stall, the recirculated air can almost be considered a closed system. Blade tip vortices from the rotor disk become trapped in this recirulation ring shape enclosing the outer rim of the rotor disk. If additional blade pitch angle is added, corresponding to an increase in collective, the rotor only recirculates the closed system blade wash at an increasing rate.

Theoretically, the vortex ring state begins at rates of descent just below hover and transitions into the windmill brake state. From a practical standpoint, extreme flow variations do not start until the rate of descent is about half the hover induced velocity. Hover induced velocity is that downwash velocity which occurs when rotor thrust equals the gross weight of the aircraft.

A well defined slipstream ceases to exist as an aircraft begins to descend. The region from descent to the windmill brake state can be referred to as the vortex ring state. A more commonly accepted value at which onset of the vortex ring state occurs is when the rate of descent equals 0.7 times the induced velocity at hover.

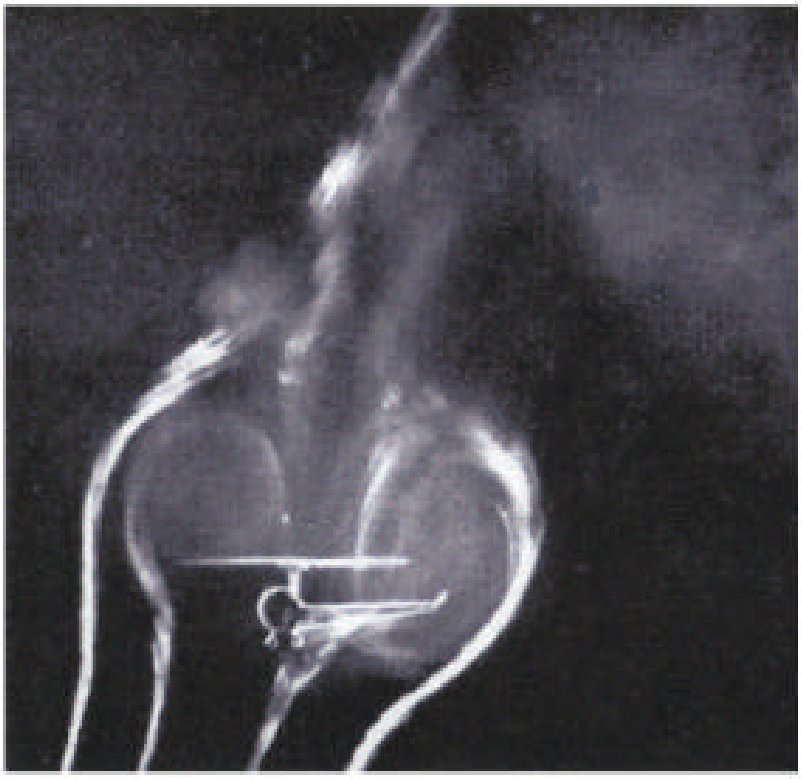

Figure 2. Recirulation During Flight in the VRS.
[From: Drees and Hendal Film, 1951]

The vortex ring state has been of concern to the designers of helicopters since the 1950’s. This phenomenon was first recognized by George de Bothezat in 1922. Early studies to verify the existence and its effects yielded results that are consistent with today's data.

Rotor operations in the vortex ring state will cause some of the most violent aircraft vibrations of any flight regime. Flight conditions are characterized by high rates of descent, extreme vibrations, and temporary loss of control. Flight profiles where the vortex ring state is typically encountered include steep approaches, approaches with a tail wind, or conditions where engine power is

limited. The vortex ring state can also be encountered during aggressive maneuvering flight where flow velocities are normal to the rotor disk plane.

Among different aviation communities the term vortex ring state can be referred to by several different meanings. In Naval Aviation, the vortex ring state is referred to as “power settling.” This phenomenon should not be confused with the flight profile “settling with power,” which often refers to situations where power required exceeds power available. However, this condition can evolve into encounters with the vortex ring state. When used in this thesis, the term power settling refers to the vortex ring state.

3. The Windmill Brake State - Autorotation

As the rate of descent is increased, the flow up through the rotor increases. When the value of this flow up through the rotor reaches a value twice that of the hover induced velocity, the rotor is considered to be in the windmill brake state. The rotor is now extracting energy from the high velocity slipstream. The rotor disk can be thought of as an effective parachute, Figure 1. In fact, Gessow and Myers [Gessow, 1952] show that the lift force generated by a rotor in autorotation is equivalent to that produced by a parachute of the same diameter as the rotor.

THIS PAGE INTENTIONALLY LEFT BLANK

II. ANALYTICAL AND EXPERIMENTAL MODELS OF THE VORTEX RING STATE

A. FUNDAMENTAL MOMENTUM THEORY

Momentum theory and blade element theory are used to analyze rotor performance in a hover, climb and descent. Momentum theory applies the basic conservation laws of mass, momentum, and energy. Blade element theory predicts the actual forces acting on an element of the rotor blade as a result of its motion through the air. Figure 3 displays the basic steady flow parameters and the funneling effect.

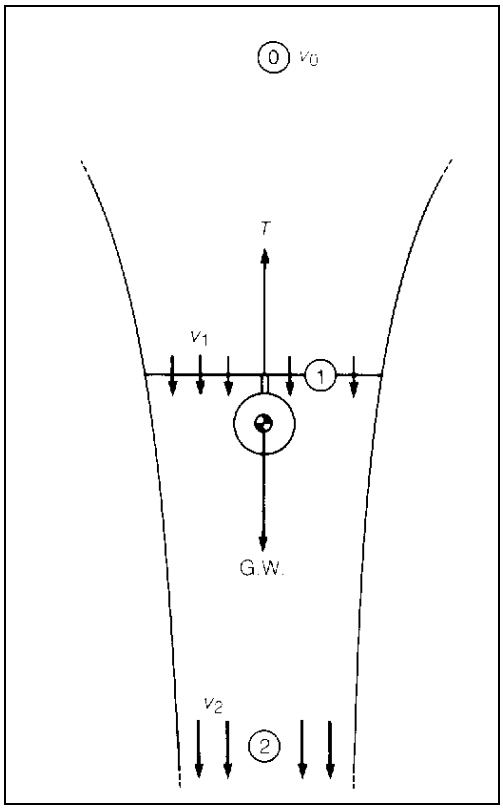

Figure 3. Flow Field Condition. [From: Prouty, 1986]

The rotor is modeled as an actuator disk with zero thickness that supports a pressure differential and accelerates air. The velocity V_1 is located at the rotor plane and V_2 is at a point below the rotor, as in Figure 3. Mass flow through the rotor system is given as:

$$\dot{m} = r A V_1$$

Where r is the density of air (associated constant) and A is the area swept out by the rotors. The thrust T produced by a rotor system is a product of the mass flow $\dot{m}$, and the change of velocity of the air mass ΔV.

$$T = \dot{m} \Delta V$$

Assuming the air far above the rotor v_0 has no velocity, ΔV is simply V_2. Then rotor thrust is given as:

$$T = \dot{m} V_2 = r A V_1 V_2$$

Kinetic energy, KE, is imparted as the air mass passes through the rotor.

$$EnergyRate = Force(T) \times Velocity(V_1)$$

The change in kinetic energy is the rate energy is imparted to the downstream wake. The change in kinetic energy across the entire system is simply the kinetic energy at region 2. The rate at which energy is imparted to the flow stream by the rotor must equal the rate at which kinetic energy is generated in the wake.

$$[\frac{dKE}{dt}]_{wake} = \frac{1}{2}\dot{m}V_2^2$$

Setting the two equations equal:

$$\dot{m}_1 V_1 V_2 = \frac{1}{2}\dot{m}_2 V_2^2$$

Considering a closed system, the mass flows are equal, due to continuity. Leaving the following expression:

$$V_2 = 2V_1$$

Substituting this back into the thrust equation reveals the following equation for hover induced velocity:

$$V_h = \sqrt{\frac{T}{2rA}}$$

This equation has been derived assuming a uniform flow field cross section. Rotational energy induced by torque from the rotor is neglected. The purpose of blade twist is to produce a more uniform flow field across the rotor disk. Anything other than uniform flow through the rotor plane increases the kinetic energy for the same momentum value and is less efficient.

1. Vortex Ring State

Momentum theory remains valid until the flow field begins to breakdown and become unsteady, as in VRS. This can occur at a moderate rate of descent, 500-700 feet per minute. The flow in the recirculated wake becomes difficult to analyze. When the rate of descent reaches the hover induced velocity there is analytically no mass flow through the rotor. Because of this fact, empirical data from instrumented rotor systems is used to obtain performance results. Momentum theory no longer is valid during

operation in the vortex ring state because of the ambiguity in defining a control volume where the governing equations can be applied.

2. Autorotation

Autorotation is considered to occur at the boundary of the vortex ring state. That is, ideal autorotation occurs when the rate of descent equals twice the hover induced velocity. During power-off descent the source of power rotating the rotorhead is the air flowing upward. The lift vector of the blade element is equal to the drag component. Using blade element and momentum theory, an approximation for rate of descent during an autorotation is $V_D \approx 2[V_h]$.

3. Windmill Brake State

At very large rates of descent the rotor is extracting power from the air flowing upwards through the rotor. Momentum theory can be applied to determine rotor performance when operating in the windmill brake state with a clearly formed slipstream.

B. WOLKOVITCH

Dr. Julian Wolkovitch published a paper in the *Journal of the American Helicopter Society* in 1972 entitled "Analytical Prediction of Vortex Ring State Boundaries for Helicopters in Steep Descents." He used momentum theory, supported by empirical data, to predict the upper and lower boundaries of the vortex ring state.

The vortex that forms around the circumference of the rotor disk during a vertical descent was used to calculate an average value for the velocity located at the core of the vortex. Wolkovitch defined the upper boundary of the vortex ring state when this resulting velocity, acting at the core, equaled zero. When the vortex core has no

movement away from the rotor plane, unsteady flow will occur. This was calculated to be the critical descent velocity (V_{crit}) at which the vortex ring state occurred.

The critical descent velocity was also greatly dependent upon rotor blade tip loss that occurred due to non-uniform lift distribution across the blade. Lift rapidly decreases across the span near the tip of the blade during encounters with the vortex ring state. This results in a corresponding loss of induced flow through the rotor and decreases the effective radius of the rotor system.

To substantiate his results, Wolkovitch used experimental data showing thrust fluctuations indicating unsteady flow when operating in the vortex ring state. His results showed significant thrust fluctuations at approximately $V_{crit} = 0.7V_h$. He reported mean-to-peak thrust fluctuations of 14 percent of the mean thrust, as shown in Figure 4.

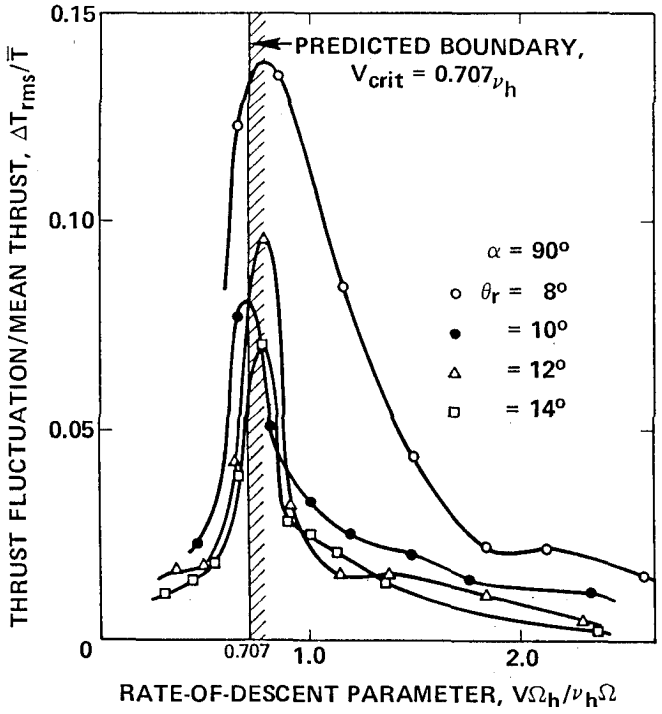

Figure 4. Measured Thrust Fluctuations During a Vertical Descent. [From: Wolkovitch, 1972]

The windmill brake state occurs when the descent rate is increased to a point where the steady flow reappears. This defines the lower boundary of the vortex ring state. The entire rotor wake now exists above the rotor plane. Wolkovitch suggest that the lower boundary is not as well defined as the upper and therefore uses an empirical factor to account for the contraction of the wake above the rotor during descent.

Wolkovitch compares his calculated boundaries to that obtained from flow visualization, Figure 5. It is apparent that the upper and lower boundaries do not merge as airspeed is increased, implying that vortex ring state can be encountered at high airspeeds.

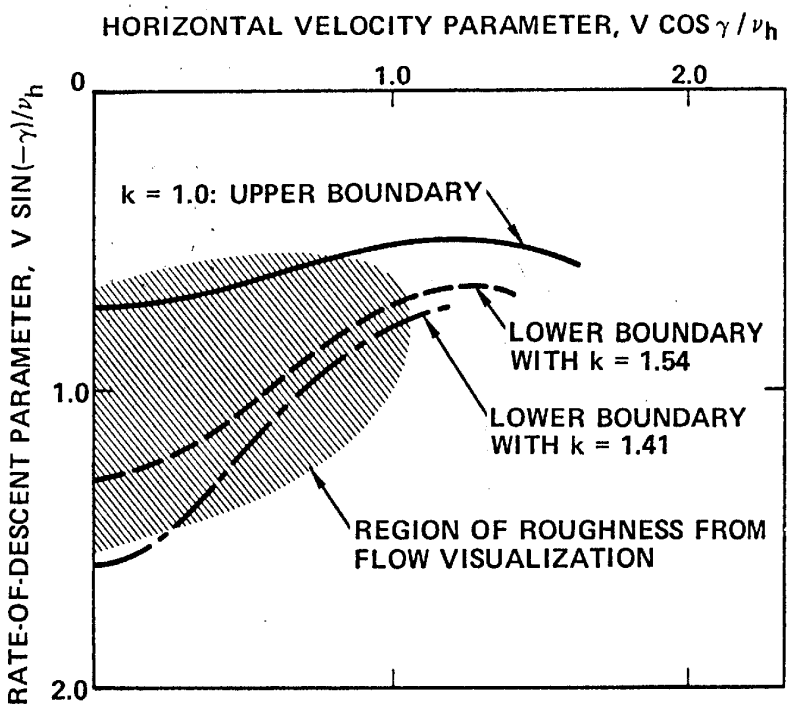

Figure 5. Calculated VRS Boundaries Compared to Flow Visualization Boundaries. [From: Wolkovitch, 1972]

C. PETERS AND CHEN

Drs. David Peters and Shyi-Yaung Chen published a paper in the *Journal of the American Helicopter Society* in 1982 following up on Wolkovitch's work but using a more consistent wake model. [Peters, 1982] They refer to the hover condition when the rotor's induced flow is imparting energy in to the flow field and the windmill brake state as extracting energy.

They took into consideration the horizontal component of velocity generated by forward flight. They derived an equation that relates the normalized rate of descent h, horizontal velocity m, and hover induced flow V_h.

$$h = V_h \pm \sqrt{\frac{1}{V_h^2} - m^2}, \qquad v_i m \leq 1$$

Peters and Chen conclude that during high values of inplane flow, the vortex ring state does not occur. [Peters, 1982] They conclude that there is a vortex ring state boundary at a determined forward airspeed specified by a maximum normalized inplane horizontal velocity.

From actual flight data there is clearly a maximum inplane velocity for which the vortex ring state dissipates. Increasing forward airspeed is a typical recovery technique from the vortex ring state. The unsteady air formed around the rotor tips is swept aft and above the aircraft. With consideration of inplane velocity, the subsequent equations give rise to a more defined boundary for the vortex ring state, Figure 6.

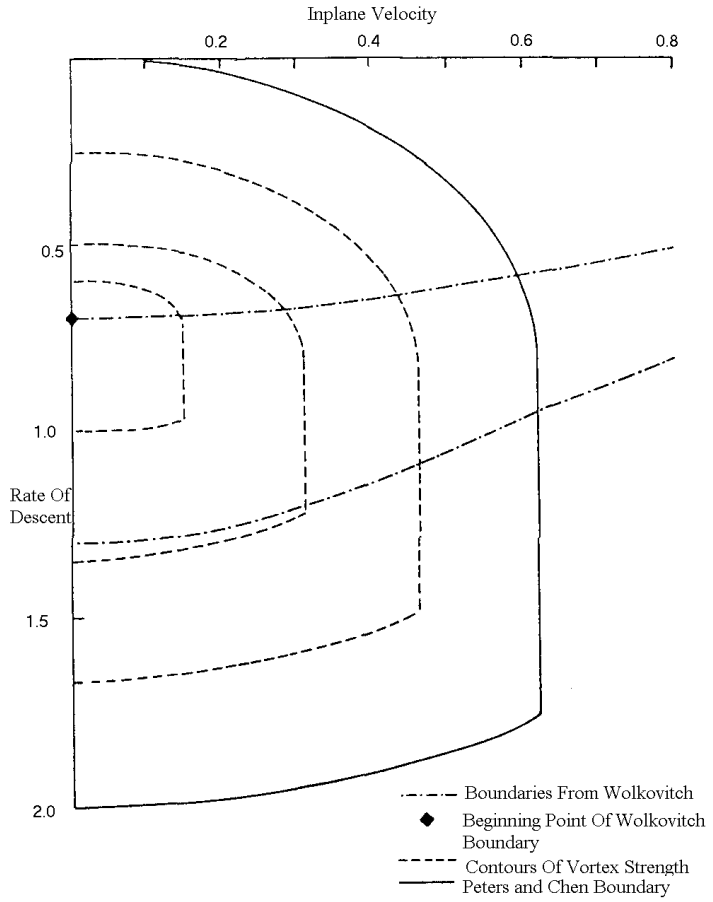

Figure 6. Peters and Chen VRS Boundary. [From: Peters, 1982]

Peters and Chen showed that there is a boundary for the vortex ring state at a normalized inplane forward velocity and proved the general boundary was larger than predicted by Wolkovitch. They also determined that the center, not the edge of the region is located at normalized rate of descent of 0.707.

D. GAO AND XIN

Gao and Xin published a paper in the *First Russian Helicopter Society Annual Forum Proceedings* in 1994 entitled "An Experimental Investigation into the Vortex Ring State Boundary."

Goa and Xin's primary concern was to eliminate the common wind tunnel limitations, interference flow interaction at the tunnel walls causing boundary layer interference, and the poor low speed characterists of wind tunnels. The disturbed air surrounding the rotor during the vortex ring state can extend out a distance of several rotor diameters. Therefore, the interaction with the tunnel walls can be substantial.

They used a whirling beam device capable of measuring torque and thrust with a strain gauge. Output from the strain gauge was amplified and sampled. They tested three different airfoils with varying twist and chord.

Gao and Xin used a semiemperical approach and momentum theory to determine new boundaries of the vortex ring state. They experimentally determined that the boundary occurs when the free stream velocity reaches a critical value of $0.28V_h$. Descent velocities 0.6 to 0.8 times the hover induced velocity ($0.6\,V_h < V < 0.8\,V_h$) is identified to be the region of most sever encounters with VRS. Data indicated drastic fluctuations in torque and thrust during operation in the VRS region, Figures 7 and 8.

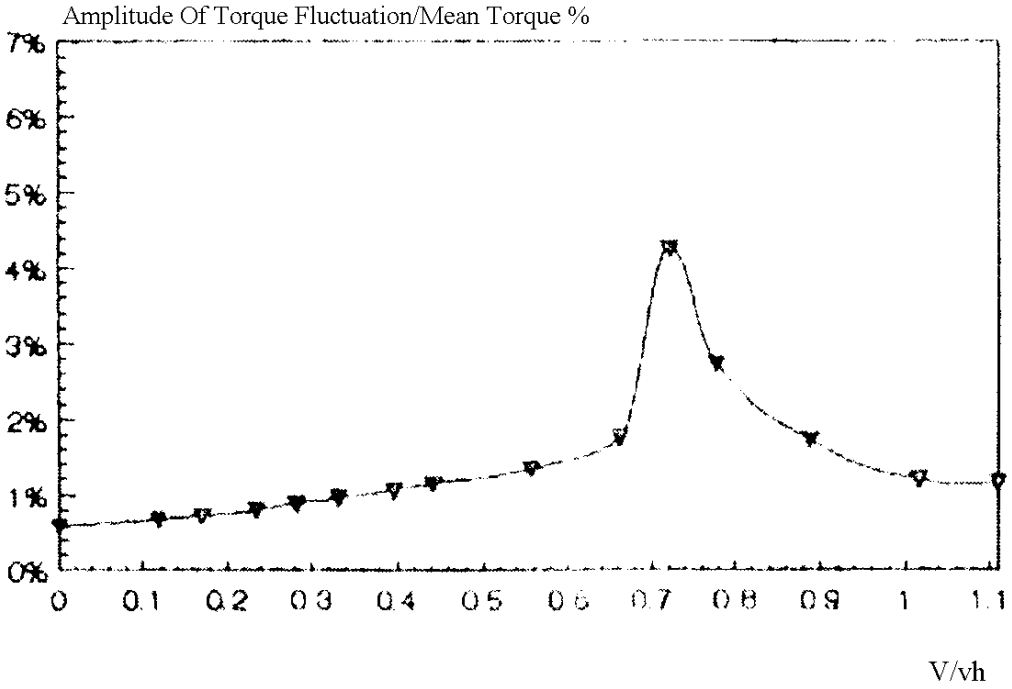

Figure 7. Torque Fluctuations During Vertical Descent. [From: Gao And Xin, 1994]

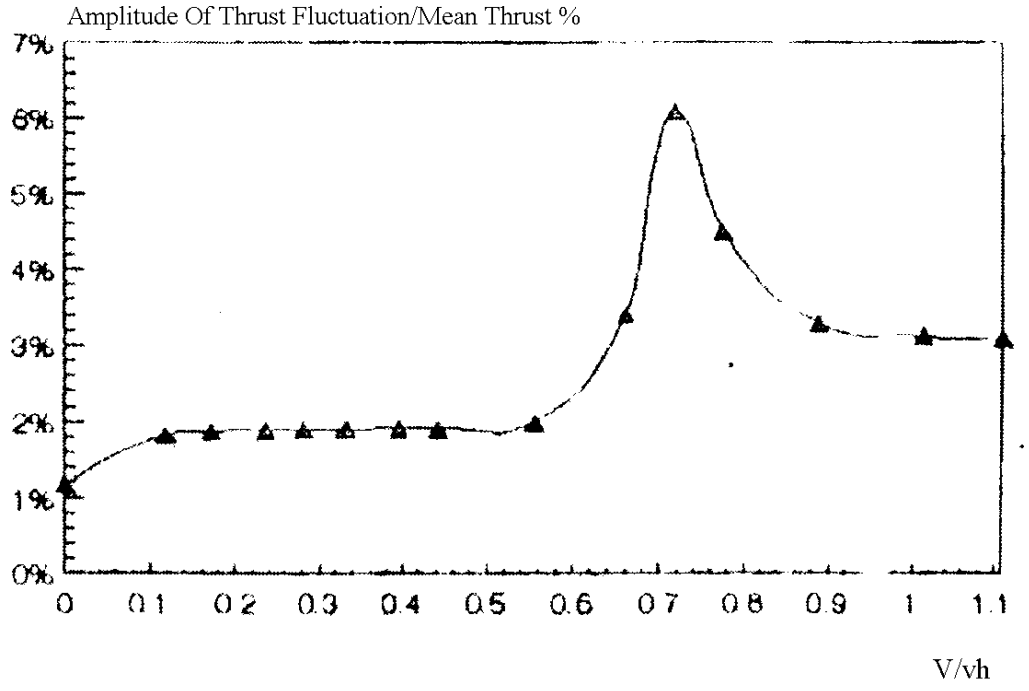

Figure 8. Thrust Fluctuations During Vertical Descent. [From: Gao And Xin, 1994]

A significant discovery was the correlation of mean torque to descent rate; they called this the power settling phenomenon. The “bucket” torque setting can easily be seen in Figure 9 at a descent rate of V=0.28V_{hover}. Beyond this point it requires an increase in mean torque to descend at a faster rate. Above V=0.8V_{hover} Gao and Xin predict the increase is due to local blade stall. Although, above descent rates greater than V=0.8n_{hover} the torque fluctuations decrease as the rotor system transitions into the windmill brake state. They found that the lowest descent rate where the vortex ring state can be encounter is V=0.28n_{hover}. Therefore, this value is defined as the critical descent velocity, V_{crit}=0.28V_{hover}.

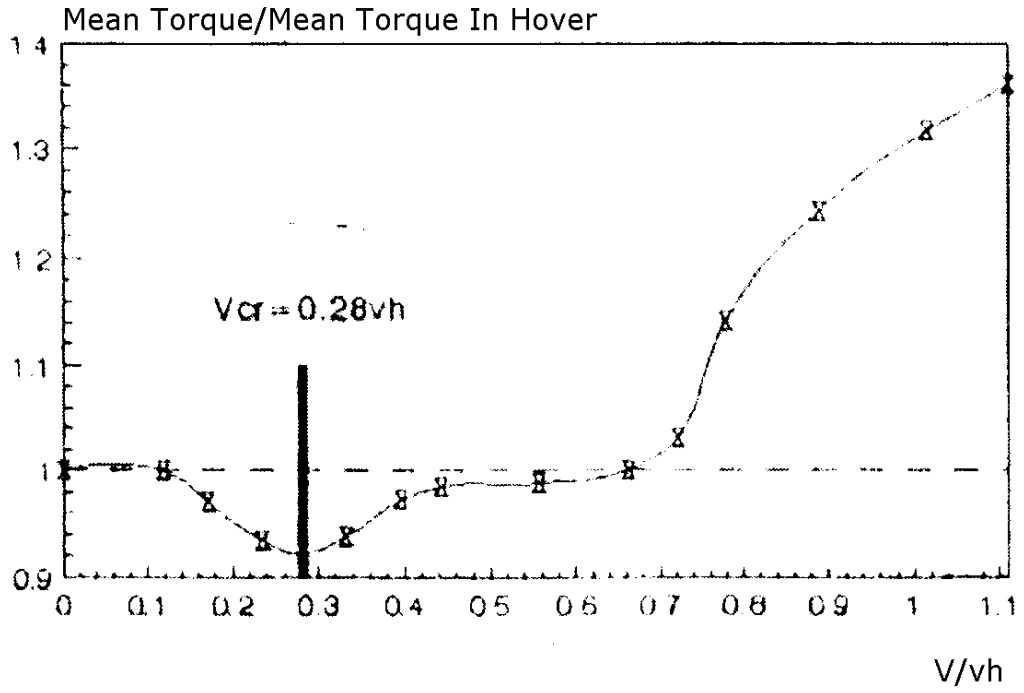

Figure 9. Mean Torque During a Vertical Descent. [From: Gao And Xin, 1994]

Gao and Xin determined for their rotor system, that the vortex ring state is encountered only for steep approaches of greater than 70 degrees.

All three models are displayed in Figure 10.

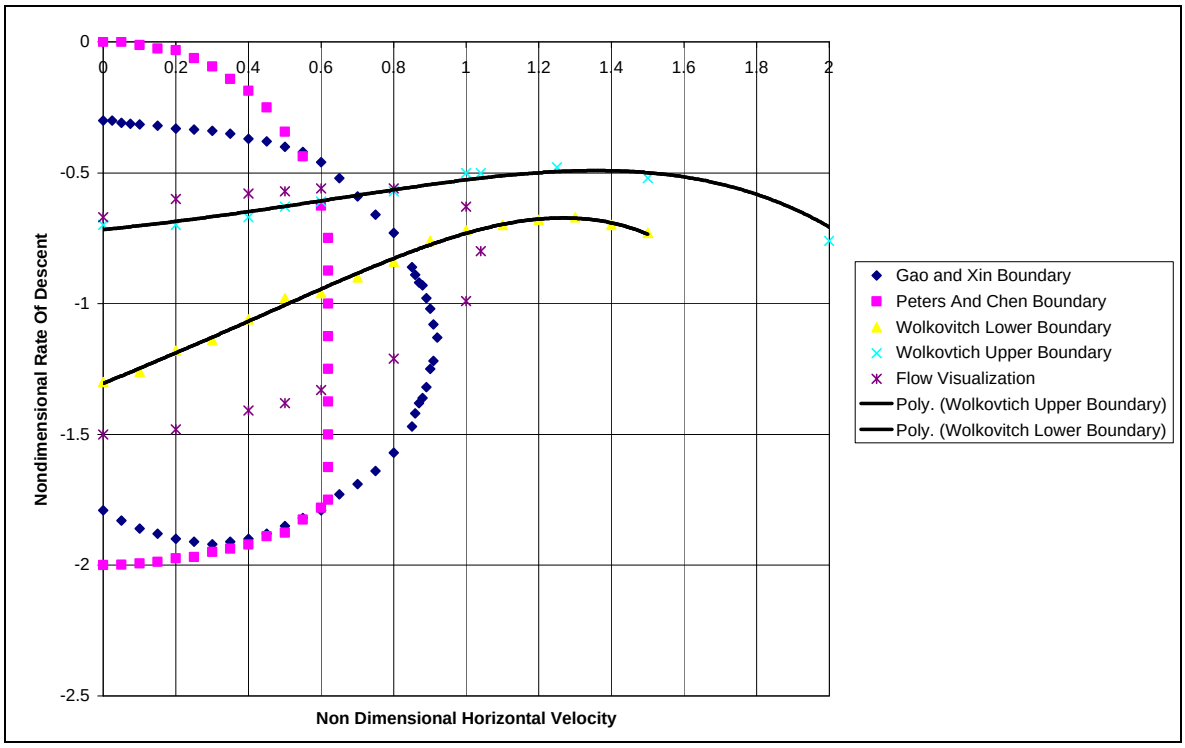

Figure 10. Superposition of Vortex Ring State Boundaries and Flow Visualization. [From: Varnes, 1999]

E. ENGINEERING MODEL

Several recent analytical models for predicting the flight boundary of the vortex ring state have been developed. An engineering model was developed based on defining VRS development in terms of the rate of growth of the disturbances relative to the rate at which disturbances are covected downstream [Newman, 2001]. The growth of

disturbances in the flow field is proportional to the wake vorticity. The shed vortices are a direct result of rotor thrust. The engineering model uses conventional actuator disk theory to identify a rate of transport of the wake instabilities into the downstream flow field. The foundation of the theory is based on classical momentum theory. [Newman, 2001]

F. WAKE STABILITY THEORY

Using a linear analysis of the rate of growth of perturbations introduced into the wake structure can help identify the process of degeneration. The wake stability theory assumes an incompressible, irrotational fluid with embedded vorticity which will be transferred to the surrounding fluid. The stability of the rotor wake is dependent on both rotor geometry and the operating state. With this method, predicting what happens after the rotor wake has become unstable is not possible. Numerical methods must be used to reveal the non-linear formation of the unstable wake. [Brown, 2002]

G. VORTICITY TRANSPORT MODEL (VTM)

The vorticity Transport Model (VTM) developed by Brown uses a direct numerical computational solution to predict the development of the rotor wake vorticity. Using the Navier-Stokes Equation, assuming incompressibility and the limit of vanishing viscosity, shows rotor wake vorticity is related directly to aerodynamic loads on the blades. The Biot-Savart relationship is used to relate the velocity at any point near the rotor to the vorticity distribution. Aerodynamic loading on the airfoil is determined from the geometry and strength of the rotor wake. Moderate thrust fluctuations at low descent rates quickly increase as the

descent rate approaches 0.5 times the hover induced flow. [Brown, 2000] The model can represent blade-to-wake, and wake-to-wake interactions that lead to growth and rupture of the vertical wake pattern. [Brown, 2002]

H. FREE VORTEX MODEL (FVM)

The FVM is a computational method with improved computational efficiency, compared to VTM. Although, there is a loss of resolution when using FVM. A Lagranian description of flow is used to pattern the FVM. Discrete line vortices represent structure of the rotor wake vorticity. For straight line segmentation of the vorticity being shed and trailed from the blades the approach is spatially second order accurate. [Brown, 2002] Unfortunately, computational model descriptions of highly unstable, nonlinear, time dependent flow in the vortex ring state are susceptible to small perturbations and can result in rapid divergence of FVM and VTM predictions.

THIS PAGE INTENTIONALLY LEFT BLANK

III. EXPERIMENTAL APPARATUS

The analytical and experimental research presented has provided extensive understanding and further defined the boundaries of the VRS. Although published research of studies conducted in a water tunnel is very limited. It is believed that vibrational analysis of a rotor operating in VRS deserves additional investigation. In the effort of contributing to this field of research a small scale rotor was constructed to operate in a water tunnel. The apparent lack of vibrational analysis of the rotor operating in VRS has motivated this thesis.

A. WATER TUNNEL

A flow visualization water tunnel manufactured by Eidetics International was used to conduct our experiment, Figure 11. The tunnel has a 15 inch by 15 inch flow area and can produce smooth flow at speeds up to 16 inches per second.

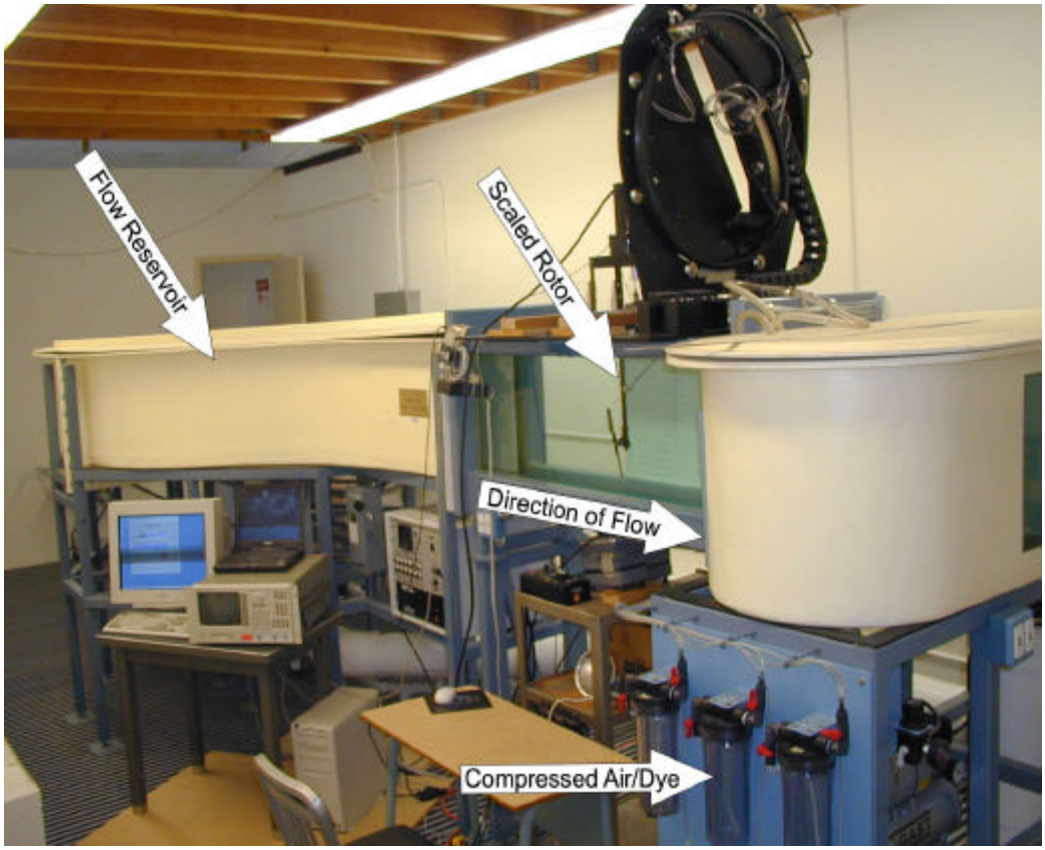

Figure 11. Flow Visualization Water Tunnel with Scaled Rotor Installed.

The advantage in using a water tunnel for this research is the ability to reduce the flow velocities compared to full scale models operating in air. The similarity of flow dynamics between water and air enable this advantage; the streamline patterns are geometrically similar and the force coefficients are the same. Distributions of parameters such as V/V_∞ are the same when plotted against common nondimensional coordinates. The flow over geometrically similar bodies at the same Mach and Reynolds numbers are dynamically similar, therefore the lift, drag, and moment coefficients are identical.

Disregarding the scaling of rotor chord length, c, comparison of Reynolds numbers associated with water and air reveals the source of the flow velocity advantage. Reynolds number calculations indicate a reduction of velocity by a factor of 15. r is density and m is the dynamic viscosity.

$$R_e = \frac{rVc}{m}$$

$$(\frac{rV}{m})_{water} = (\frac{rV}{m})_{air}$$

$$V_{water} = (\frac{m}{r})_{water}(\frac{r}{m})_{air}V_{air}$$

$$V_{water} = \frac{1}{15}V_{air}$$

Rotor tip speeds of a full scale helicopter are approximately 600 ft/sec. The chord length can range from six to eighteen inches. Therefore, Reynolds numbers of a full scale rotor blade operating in air are on the order of 10^6.

The chord length of the scaled model blade used in the present experiment is one inch. A blade tip speed of 14 ft/sec was chosen. This results in a Reynolds number in water on the order of 10^5, close to that of a full scale blade. In addition, the corresponding rotational speed provided excellent flow visualization.

B. SCALED ROTOR SYSTEM MODEL

A scaled model rotor system was constructed using the tail rotor system of a Hawk IV radio controlled hobby helicopter, Figure 12. The rotor diameter is nine inches and corresponding rotor area is 0.44 ft^2. A variable RPM

Bodine electric motor provided 1/8 horsepower to rotate the two symmetric blades at the desired speed of 360 RPM. The blade pitch angle was set at ten degrees of pitch and tunnel flow velocity was varied from one to nine in per second.

Small compressed air bubbles were injected into the flow field at the edges of the rotor plane. The air discharge nozzle was crimped to produce as small bubbles as possible. The viscosity force acting to hold the bubbles in solution countered the buoyancy force and helped keep the air bubbles from being forced to the surface. Two air outlet probes were placed at points with very close clearance to the rotating blades. Each passing blade picked up the injected air and formed a flow field of small bubbles.

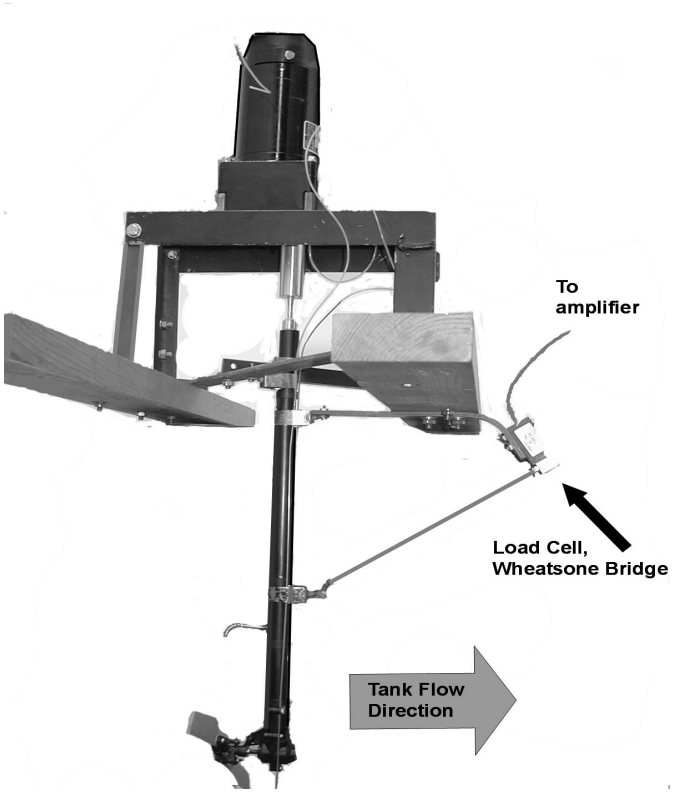

Figure 12. Rotor System Device.

C. DATA ACQUISITION

For static measurements a Wheatstone bridge strain gauge load cell was connected to a meter, and provide a visual output display of the thrust load. The load cell was attached as shown in Figure 12. Calibration was accomplished with static weights prior to each experiment.

The same Wheatstone bridge strain gauge was used to measure dynamic forces on the rotor system. The load cell signal was feed to an Ectron model 563H amplifier. 5 Vdc excitation voltage was provided by the amplifier to the Wheatstone bridge. A Hewlett Packard 35665A Dynamic Signal Analyzer was then used to compute power spectra from the thrust data, Figure 13. All data were low pass filtered at bandwidth 64 Hz and sampled at 128 samples per second for 2 seconds. Four time records were (rms) averaged with 0% overlap. The display was 0 to 50 Hz with a frequency resolution of 0.5 Hz. A Hanning window was used. The Nyquist criteria was met by sampling more than twice as fast as the highest frequency component displayed on the analyzer.

Figure 13. Ectron 563H Amplifier and Hewlett Packard 35665A Dynamic Signal Analyzer.

IV. EXPERIMENTAL RESULTS

A key factor in accurately predicting the aerodynamic behavior of a rotor system is an improved understanding of the wake distribution generated by the rotor system. The understanding and eventual prediction of wake dynamics during descending flight is key to improved understanding of the phenomenon of the vortex ring state.

A. HOVERING CONDITIONS

A helical vortex wake can be seen forming downstream of the rotor blades in Figure 14. The rotor system is producing thrust to the right and can be visualized as a helicopter in flight by rotating the image 90 degrees counterclockwise. Images were captured using a digital still camera with a fast shutter speed setting of 1/320 sec. When the flow in the tunnel is turned off, the flow visualization section becomes a closed system with no area for rotor wash to dissipate. This made simulating hover conditions impossible without a slight flow velocity established in the tunnel. When a slight tunnel flow velocity of three inches per second was turned on, the rotor wash was able to displace naturally. The rotor device was installed during this test so the flow was from above, if the rotor device was viewed as a hovering aircraft (from the right of the rotor in the photos). This can be thought of as a climb profile.

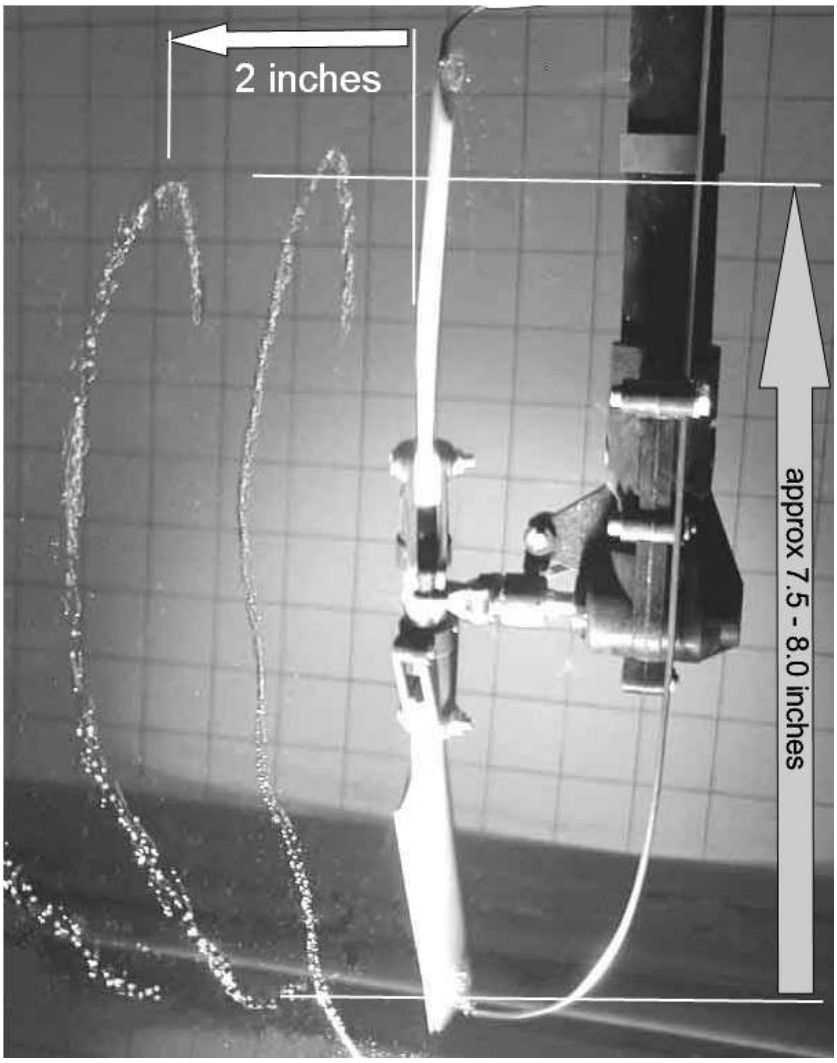

Figure 14. Helical Vortex Wake in a Climb. Note Wake Contraction.

1. Momentum Theory Validates Observation

In Figure 14 the rotor was operated at 360 RPM (6 Hz) with blade pitch set at ten degrees. In addition to the rotor producing thrust, and shedding the helical wake downstream, an additional water tunnel flow rate exist from right to left in the photo. The velocity, V_{wake}, in the wake at a position approximately one inch downstream of the

rotor was obtained from the photograph by $V_{wake} = \frac{\Delta x}{\Delta t} = \frac{2in}{0.17} = 12\ in/\sec$, where Δx is the measured distance from the bubbles entrained in the core of a helical vortex at a position corresponding to one cycle elapsed and Δt is the time for one cycle of rotation. This velocity equals the sum of the climb induced velocity through the rotor, V_{ic}, and the water tunnel flow velocity, $V_c = 3\ in/\sec$.

The tunnel flow enabled the rotor wash to be convected downstream, and to establish a well-defined flow field such as shown in Figure 1, and for which momentum theory applies. The tunnel flow velocity of 3 in/sec can be thought of as a rate of climb, V_c.

A load cell thrust measurement (T) during this observation was recorded as 0.5 lb. A hover induced velocity (V_h) is calculated for this specific thrust value:

$$V_h = \sqrt{\frac{T}{2rA}}$$

$$= \sqrt{\frac{0.5lb}{2(1.95\frac{slugs}{ft^3})p\,(\frac{4.5in}{12\,ft})^2}}$$

$$= 6.5\ in/\sec$$

Using momentum theory the following equation gives the induced velocity for this climb condition. [Prouty, 1986]

$$V_{ic} = -\frac{V_c}{2} + \sqrt{\left(\frac{V_c}{2}\right) + V_h^2}$$

$$= -(\frac{3in/\sec}{2}) + \sqrt{\left(\frac{3in/\sec}{2}\right) + (6.5in/\sec)^2}$$

$$= 5.0\ in/\sec$$

The velocity through the rotor is, then $V_{ic} + V_h = 8\ in/\sec$.

Conservation of mass between the rotor and the wake downstream requires $A_{rotor}(V_{ic} + V_h) = A_{wake}V_{wake}$. Taking $A_{rotor} = 0.44\ ft^2$ and $(V_{ic} + V_h) = 8\ in/\sec = \frac{2}{3}\ ft/s$ the left hand side is calculated to be approximately 0.29 ft^3/sec.

The diameter of the wake where the velocity was estimated is estimated to be approximately 7.5 – 8.0 inches. This results in an estimated wake area $A_{wake} = 0.33\ ft^2$. With the estimated value of $V_{wake} = 12in/\sec$, The right hand side of the mass conservation equation is estimated to be approximately 0.33 ft^3/sec, a difference of only 10% from the left hand side. This should be considered a remarkable agreement, and shows that momentum theory can be used to adequately describe the gross features of the flow in this experiment.

Momentum theory predicts a rapid wake contraction downstream of the rotor, which is clearly apparent in Figure 14. Theory further predicts that the area of the wake very far downstream of the rotor should be ½ the rotor swept area. From measurements taken off the photograph of Figure 14, we observe that, at a position two inches

downstream of the rotor, the diameter of the wake is approximately seven inches, and the wake area relative to the rotor swept area is already $\frac{(7)^2}{(9)^2} = 0.6$

B. VORTEX RING STATE

Throughout the experiment the rotor was operated at a constant 360 RPM with a blade pitch angle of ten degrees. With these parameters, the hover induced velocity was estimated by visually observing when the helical vortex wakes collapse in the plane of the rotor. The water tunnel flow velocity was increased until this occurred, Figure 15.

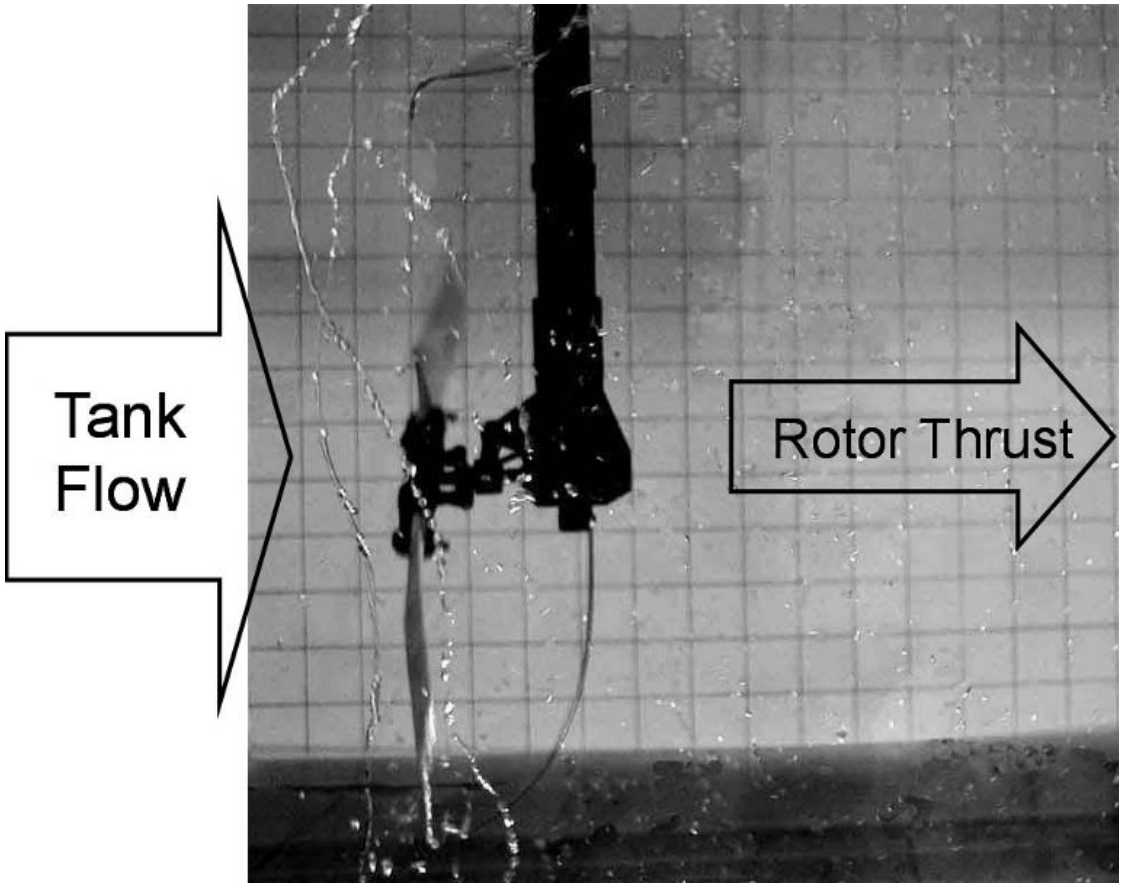

Figure 15. Collapsing Vortices, Impending VRS with Flow Rate at 4.5 In/Sec.

The average thrust measurement when the vortex wake collapsed was recorded as 0.7 lbs. A corresponding velocity is calculated which can be considered as a hover induced velocity with a thrust measurement of 0.7 lbs.

$$V_h = \sqrt{\frac{T}{2\,r\,A}} = \sqrt{\frac{0.7lb}{2(1.95\frac{slugs}{ft^3})p\,(0.375\,ft)^2}} = 4.5\frac{in}{\sec}$$

The collapsing of the helical vortex wake structure into the plane of the rotor indicates the onset of the vortex ring state. Recirulation of the rotor wake began at this point, Figure 16. The test also showed some water tunnel “wall effects” due to constraints of the small flow section of the water tunnel.

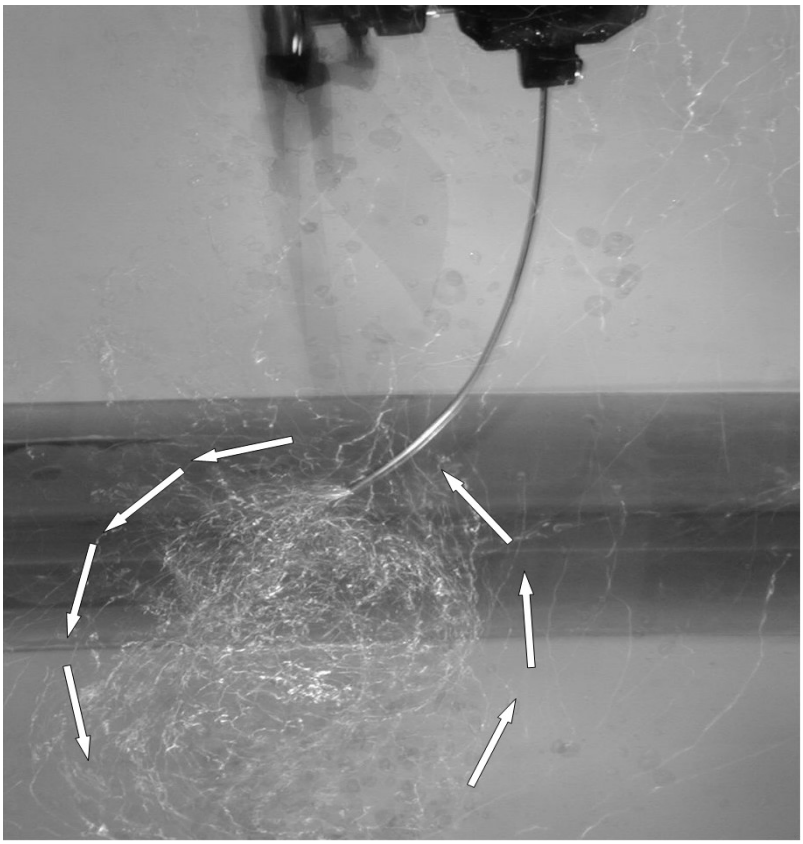

Figure 16. VRS Recirulation Take at Slow Shutter Speed.

C. TRANSITION TO AUTOROTATION

As the flow velocity of the tunnel was increased beyond 4.5 in/sec the vortices reformed on the opposite side of the rotor, the upstream side. There was a clear transition from VRS into autorotation. A helical vortex wake flow pattern, similar to that seen in a hover, reformed on the opposite side (upstream) of the rotor system. This would compare to the wake forming above a helicopter during an autorotation. A clear transition from hover through VRS and then into autorotation was achieved by gradually increasing the water flow velocity in the tunnel.

D. VIBRATION ANALYSIS

In flight, the primary indicator of the vortex ring state in flight is the associated increase in airframe vibration levels. Erratic thrust fluctuations and irregular blade flapping cause the increased airframe vibrations. Once fully operating in the vortex ring state the vibration levels are the most severe encountered in any flight regime.

A paper published by John E. Yeates in 1958 at NASA Langley explored the vibrational effects and subsequent rotor blade stresses produced during operation in the vortex ring state. A tandem rotor aircraft, with three blades on each rotor, was used in the testing. Sensors attached on the front and rear masts measured vertical vibrations. 95% of the vibratory response was reported at three times the operating frequency (3P). Although, instrumentation was not onboard to record individual harmonics during operation in the vortex ring state. [Ref. Yeates, 1958]

The vortex ring state can be viewed as a form of wake instability. In a descent, the random aerodynamic excitation builds up. As the instabilities reach the rotor plane they begin to effect the aerodynamic section loading across each airfoil. Operation in this adverse condition of VRS does not allow the downwash to convect away from the rotor. Instead, the vortex wake accumulates in the plane of the rotor. As blade vortex interaction repeatedly occurs due to unsteady blade air loads, the result is increased airframe vibrations.

1. Experimental Vibration Results

It was found that the increase in amplitude of higher harmonic frequency variations of thrust were a good indicator of impending vortex ring state. In this experiment the rotor operating speed was 6 Hz (1P), on a two-bladed rotor system. As the vortex ring state was encountered, higher harmonics of the blade passage frequency began to increase in amplitude. The content of the thrust frequency input at higher than n/rev (where n equals the number of rotor blades) is found to be a significant feature to the vibration spectrum associated with operation in the vortex ring state. “One per rev” (1P) content of thrust variation is primarily driven by cyclic pitch and resultant blade flapping. It was found to be relatively invariant to impending VRS and therefore is not a good indicator.

In preparation for data collection, a vibration shaker test was conducted on the rotor device to determine its natural frequencies. Results of the shaker test indicated that natural resonant frequencies appeared to be above the

test bandwidth of 50 Hz. Although this test was not conducted in the water, it is believed that conditions when in the water would tend to dampen natural resonances.

The experiment was conducted while operating the rotor at a constant 6 Hz rotational rate. The flow in the tunnel was gradually increased to 4.5 inches per second, where the helical vortex wake collapsed into the plane of the rotor. Continual operation in this state was possible. The visually recirculating flow field was a clear indication of operation in the vortex ring state.

Thrust data recorded during VRS, presented in the frequency domain, clearly indicates the increase in strength of higher harmonics. The blade passage frequency is defined as n times the operating frequency, P, where n is the number of blades, i.e., 2P (12 Hz) in the case of a two bladed rotor. The even multiples of the blade passage frequency, 4P (24 Hz) and 6P (36 Hz), are shown to increase during VRS, Figure 17. This response is expected as blade vortex interaction increases, causing increased variations in the section aerodynamic loading.

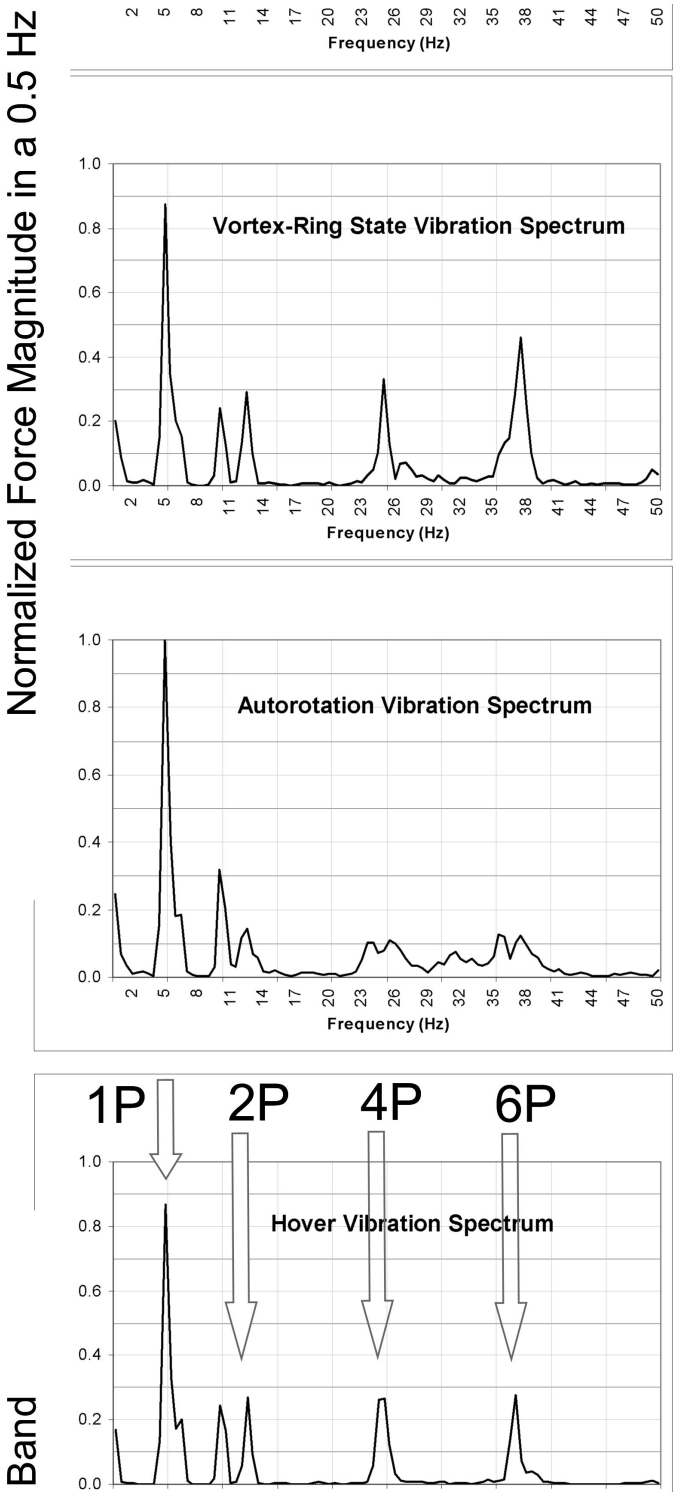

Figure 17. Scaled Vibration Spectrum from Hover (0 In/Sec), VRS (4.5 In/Sec) and Autorotation (9 In/Sec). All Are Plotted Against Same Vertical Scale, Which Is Normalized to the 6 Hz Autorotation Peak.

Note that significant hub vibration response only occurs for frequencies in the vicinity of the rotor rotation frequency (1P) and at even multiples of the blade passage frequency (2P). This is expected behavior. Rotating blades produce a vertical force at the root of the blade which results in a vertical excitation of the hub. 1P (one times rotation frequency) is primarily driven by cyclic pitch or can be a result of out of balance blades, most likely the cause in our data. Assuming all blades see the same loading at the same azimuth, only even multiples of nP frequency will be transmitted through to the fixed system, the fuselage, or hub attached to the support structure in our case. [Prouty, 1986]

Vibrations of the airframe at even multiples of n/rev are a result of (n-1), n and (n+1)/rev loads in the rotor system, which are filtered through the rotor as n/rev. (n) is the number of blades on the rotor. Harmonics of the airfoil loading cause this response. This corresponds to 2P, 4P, and 6P present in the fuselage of a two blade rotor. For example, the 4P frequency in the fuselage, or hub, is a result of 3P, 4P and 5P loads in the rotor system.

The splitting in the peaks in the hub vibration power spectra (Figure 17) is not expected, and the cause is not understood. It appears to be of the form of an amplitude modulation $\cos(w_{\text{mod}}t)\cos(wt) = \frac{1}{2}[\cos(w + w_{\text{mod}})t + \cos(w - w_{\text{mod}})t]$. This is indicative of a primary frequency, w, operating in conjunction with an additional modulation frequency, w_{mod}, superimposed. Therefore, in quantitatively reporting the

results of the power spectrum analysis, Table 1, the amplitudes of the split peaks were combined as the square root of the sum of the squares. Peak values at 2P, 4P, and 6P are reported, and the higher harmonics (4P, 6P) are compared to values at 2P.

	Hover	**VRS**	**Autorotation**
2P(averaged)	0.36	0.38	0.35
4P(averaged)	0.26	0.33	0.14
6P(averaged)	0.28	0.46	0.17
4P/2P	0.72	**0.87**	0.40
6P/2P	0.78	**1.21**	0.49

Table 1. Maximum Amplitudes and Comparison of Higher Harmonic Magnitudes of Harmonics Listed in Figure 17.

The data collected during hover condition are believed to be affected by the confines of the water tunnel. The inadequate dissipation of the rotor wash may have created greater blade vorticity interaction and some increase in higher harmonic vibration levels than would free field conditions. Even so, considering this result, the 4P and 6P harmonic are clearly higher during VRS.

The flow velocity was increased to nine inches per second to achieve windmill brake flow conditions. The helical vortex wake flow pattern reformed on the opposite side of the rotor system. Clear smooth flow patterns were

observed at this flow velocity of approximately two times hover induced, $2V_h$. The higher harmonics at 4P and 6P decreased in amplitude.

It should be noted that the flight profile of a full scale helicopter does not correlate exactly with this experiment. Autorotation in a full scale helicopter is initiated by sharply reducing the blade pitch angle (collective). In our experiment the operating RPM and blade pitch remain constant. As the tunnel flow velocity is increased, this increases the angle of attack and thrust loading. Data recorded during an actual autorotation would be associated with a much lower thrust loading than our corresponding data. Therefore, the amount of higher harmonics observed in the present experiment under autorotation conditions is probably relatively greater than would be observed under full scale flight conditions, compared to the VRS state.

Corresponding increase in higher harmonics during VRS would further increase if operated under full scale flight condition.

To correlate these model test results, an investigation was carried out with respect to full scale data collected by NASA in 1964. [Scheiman, 1964] Under the direction of James Scheiman, an extensive amount of in flight data were collected on a fully instrumented H-34 helicopter. These are the only full scale data ever taken where a significant number of VRS conditions were recorded. An analysis of the H-34 NASA data revealed similar results as recorded in the water tunnel experiment and are discussed in a later section.

2. Karman Vortex Street Effect

The Karman vortex street effect is here in considered, to determine its potential effect on the vibration data collected. The Karman vortex street is a regular array of vortices of alternating vorticity, convected downstream of a blunt obstacle, Figure 18. A Karman vortex street formed around the long drive shaft and transmitted transverse vibrations into the apparatus. Although the vibration amplitude from the Karman vortex street was assumed to be minimal, an analysis was conducted.

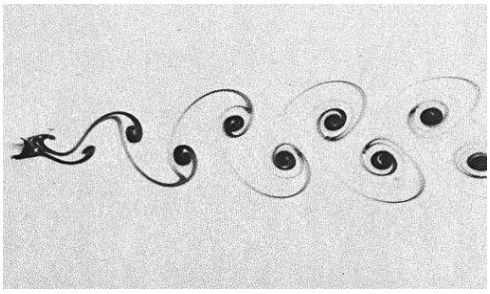

Figure 18. Karman Vortex Street Around a Circular Cylinder. [From: Van Dyke, 1982]

The Reynolds number associated with the drive shaft at a tank flow speed (V) of 4.5 in/sec is calculated. (c) is the diameter of the cowling around the drive shaft.

$$R_e = \frac{r\ Vc}{m} = \frac{(0.036\frac{lb}{in^3})(4.5\frac{in}{\sec})(0.75in)}{55.89x10^{-6}\frac{lb}{in-\sec}} = 2174$$

With $R_e = 2174$, turbulence develops soon after boundary layer separation, but the boundary layer is still laminar around the cylindrical shaft. Strouhal number is used to calculate the frequency (f) of turbulence departing the

vertical drive shaft, for a Reynolds number of 2174 the value of the Strouhal number is about 0.2. The diameter of the shaft (d) is 0.75 inches and (V) is the free stream flow velocity.

$$S_t = \frac{fd}{V} \approx 0.2$$

$$f \approx \frac{(4.5\ in/\sec)0.2}{0.75in} \approx 1.2\ Hz \qquad \text{For } 10^2 < R_e < 10^7$$

The frequency of induced vibrations due to formation and detachment of vortices is expected to be approximately 1.2 Hz.

Transverse shaft oscillations induced by the regular shedding of vortices was considered as a potential cause of amplitude modulation of the thrust variations. If this were the cause, however, we should expect to observe an increasing frequency splitting with increasing tunnel flow velocity, which we do not. Hence, we conclude that the effects of vortex shedding on the vibration spectrum are not significant.

E. AIR BODY FORMATION UNDER ROTOR DURING VRS

A peculiar phenomenon occurs as a helicopter rotor system continuously circulates air when experiencing the vortex ring state. A bubble of air forms under the rotor, which appears to grow and burst on a periodic basis, about once every second. [Prouty, 1986] This periodic dissipation causes a large scale disturbance in the surrounding flow field. The bubble erupts, causing erratic flapping in pitch and roll as rotor blades interact with this disturbed air. This unsteady turbulent air can persist until the rate of descent reaches values approximately twice the hover induced velocity.

The classic Drees and Hendal [Drees, 1951] smoke video from 1951 shows an air body that appears to form under the rotor during operation in the vortex ring state, Figure 19. This air body seems to accumulate energy and then periodically burst at intervals of one to two seconds. Reports in the literature on VRS comment that the bursting interval of approximately one second appears to be invariant to rotor size. That is, the bursting period is about the same for rotors regardless of size from model rotors up to full scale rotors.

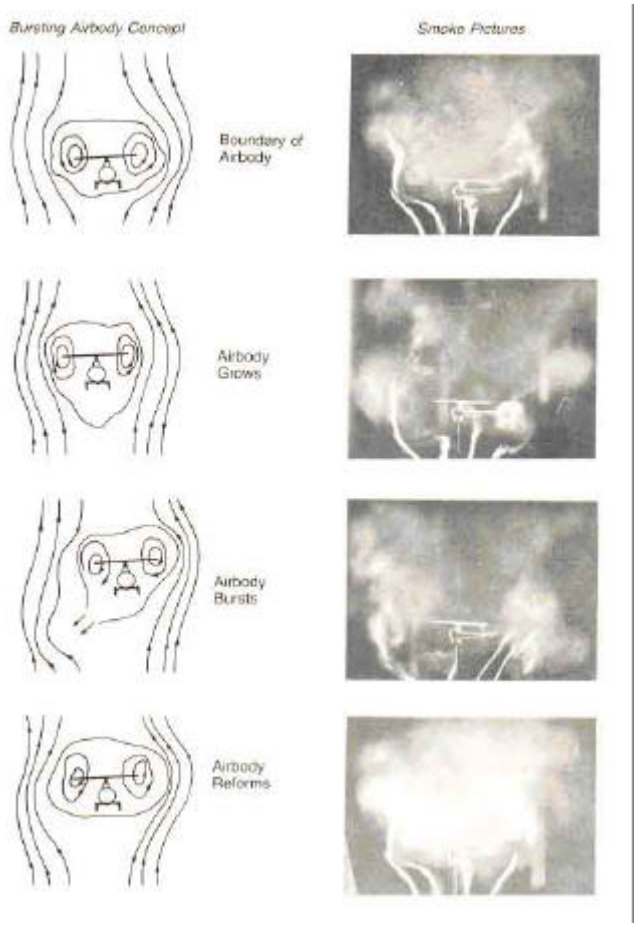

Figure 19. Vortex Ring State Air Body Formation. [From: Prouty, 1986]

The power spectrum data recorded during Goa and Xin's experiment indicated an aerodynamic fluctuation on the order of 1 Hz, Figure 20. This appears to coincide with the bursting of the air body set up under the rotor during operation in the VRS.

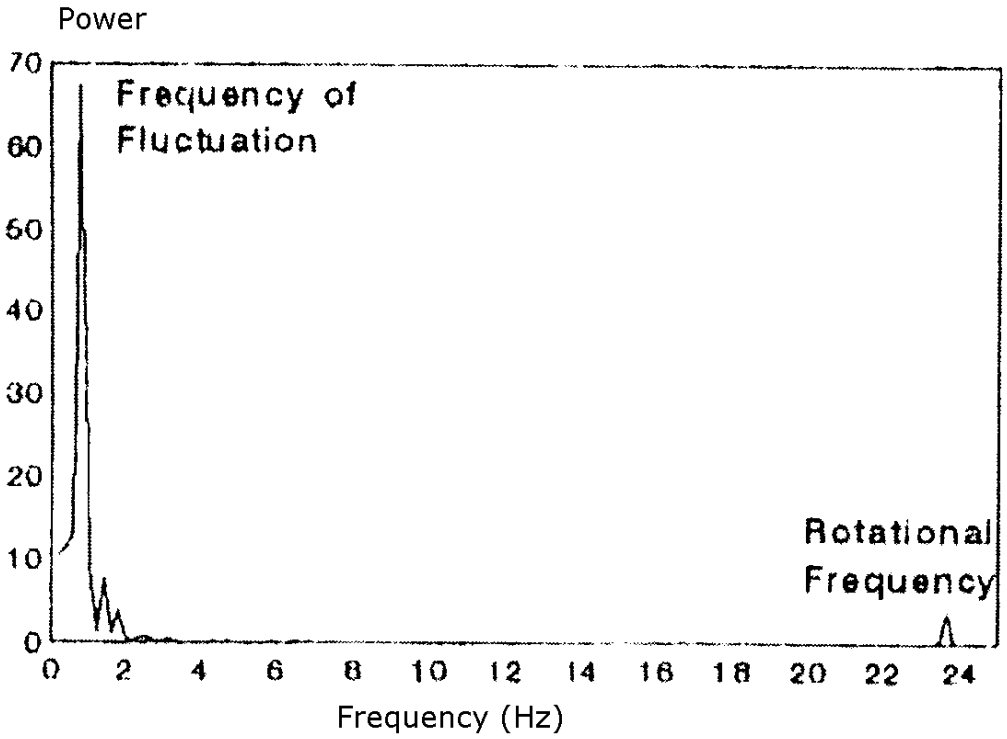

Figure 20. Power Spectrum During a Descent. [From: Gao and Xin, 1994]

During VRS conditions in the water tunnel, the same flow manifestation was observed. The phenomena manifested itself by periodic large eruptions occurring at the surface of the water at a periodic rate of 1-2 Hz, Figure 21. The formation of this air body, and its periodic dissipation, appear as though it may be a three dimensional Karman vortex street effect caused by the rotor disk acting as a solid body in the flow stream.

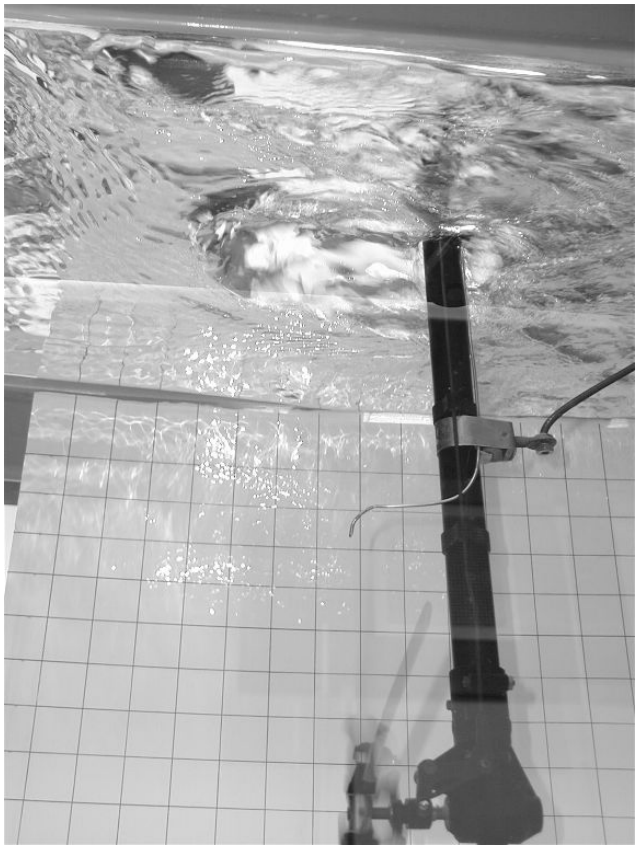

Figure 21. Periodic Surface Disturbance During VRS.

A contrasting view of normal smooth flow is during the autorotation profile as shown in Figure 22. It is clear that the periodic disturbance at the surface is no longer present.

Note, the small dip on the top right surface of the water in Figure 22 is due to the incompressibility of water and the tight operating constraints of tunnel flow area. As flow is accelerated through the rotor system, the surface is sucked down. During autorotation the rate of descent equals twice the hover induced velocity. The flow pattern is convected around the rotor and around the disk, causing a corresponding dip on the surface.

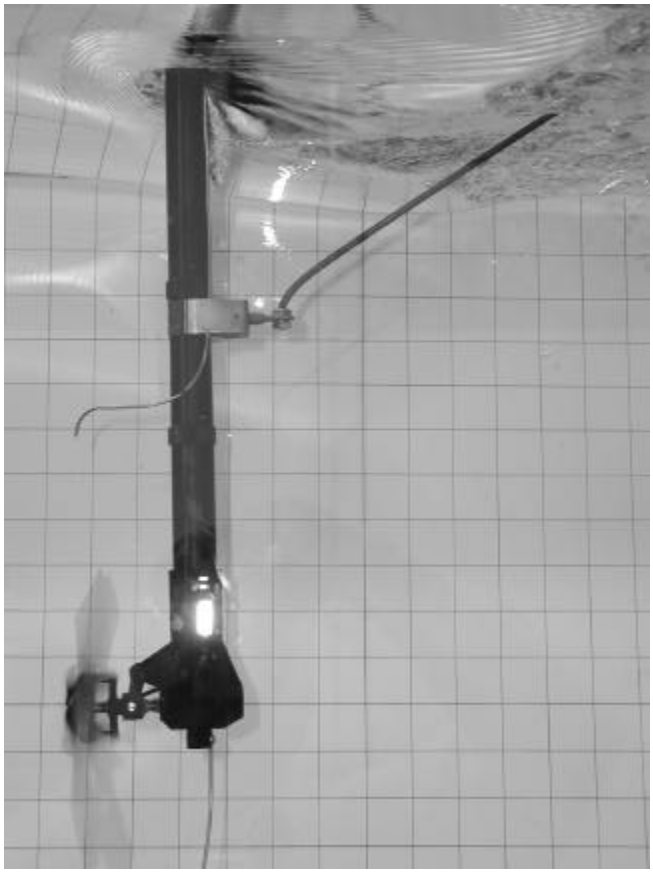

Figure 22. Smooth Flow Field.

F. V-22 BLADES

NAVAIR researcher Kurt Long at NASA Ames generously provided blades with twist similar to those on the V-22. The symmetric blades used up to this point had zero twist (i.e., constant pitch). The V-22 blades have a high degree of twist at the root of the blade and transition to zero twist at the tip. These blades were installed and tested under the same parameters as used for the symmetric blades. Thrust variation along the rotor blade, due to its pitch variation, seems to affect the hover induced velocity, as observed by the spacing of the helical vortex wake. The V-22 blades, with high twist, showed counterintuitive differences when subjected to operation in the vortex ring

state. Wake stability, affected by the thrust distribution along the blade appears to have a large effect on the descent rate boundary at which VRS is encountered. With higher rotor disk loading the boundary occurs at higher rates of descent than for a symmetric airfoil. Extensive testing of the V-22 blades was limited due to time constraints of this project but further investigation using the water tunnel promises to produce interesting new results.

V. SCHEIMAN H-34 FLIGHT TEST DATA

A. FLIGHT DATA ANALYZED

Under the direction of James Scheiman, in 1964, NASA Langley Research Center instrumented an Army Sikorsky H-34 helicopter to obtain rotor blade load distribution, flapwise bending moments, chordwise bending moments, harmonic analysis of blade root motion, and section aerodynamic loading. [Scheiman, 1964] Flight data are given for hover, climbs, autorotation, and of particular interest, partial rate of descent at slow airspeed. Additionally, there are insightful corresponding pilot comments. A comparison was made of the harmonic analysis presented in Scheiman's report with the harmonic analysis of the present experiment.

In Scheiman's study the aircraft had four rotor blades and operated at the following conditions during the selected flights listed in Table 2. Approximate gross weight was 11,500 lbs and air density was approximately 0.00216 slugs/ft^3.

Table	Flight	Forward Airspeed	Power (in Hg)	$V_{d,av}$ (ft/min)	Pilot Remarks
75	56	0	31.4	1200	Rough; blades flapping erratically; unsteady flight
79	59	8	39.3	2100	Helicopter temporarily out of control
80	59	7	40.1	1850	Helicopter temporarily out of control
84	62	6	37.4	2600	Unsteady flight
4	01	0	38.5	O	Hovering in light wind

Table 2. Scheiman - NASA Test Data.

The first four flights listed in Table 2 were specifically chosen because of the clear indications of operation near the vortex ring state. The remarks by test pilots indicating uncontrolled high descent rates, vibrations, and temporary loss of control are all typical results of operating in the vortex ring state. These comments, in conjunction with the supporting flight test data, are clear indications of operation in the vortex ring state.

1. Section Aerodynamic Loading

Aerodynamic loading data from hover flight are compared to data taken during flight in the vortex ring state. Flight number 79, encountering a descent rate of 2100 feet per minute and corresponding comments of “helicopter out of control,” is clearly encountering VRS. Data from flight 4 are from a hover, and provide a baseline for comparison. The term r/R is the radial distance along the span of the rotor blade, moving radially outward. A point at r/R=0.95 is chosen to display the load

distribution corresponding to blade azimuth, Figure 23. Azimuth, y, is in degrees of blade rotation, referenced to zero at a line extending aft along the centerline of the tail boom. In a hover, the distribution is smooth, except for a dip as the blade passes over the tail boom. In contrast, the loading associated with the VRS flight conditions exhibits drastic variations, due to blade vortex interaction.

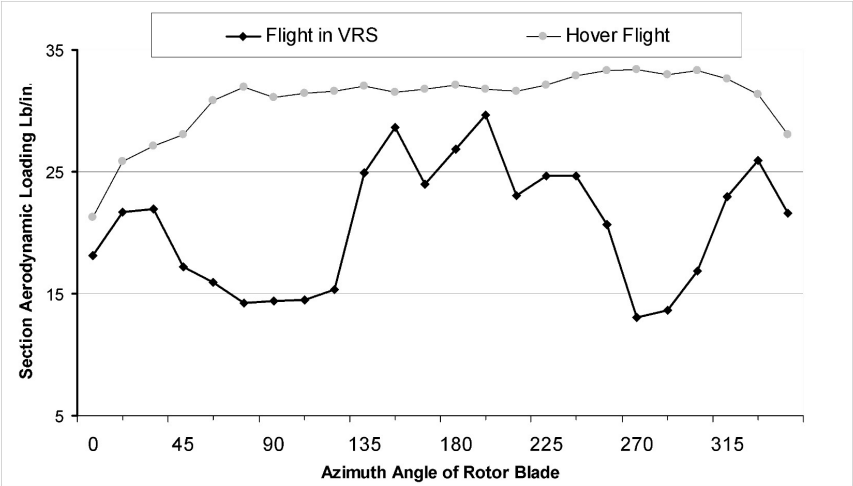

Figure 23. Section Aerodynamic Loading at R/R=0.95 as Measured in Hover and VRS at 2100 Fpm Rate of Descent.

2. Flapwise Bending Moment

Flapwise bending moment data from flights in the VRS were compared to data collected during hover. Point r/R = 0.575 was chosen to reduce some of the higher harmonic content resulting from the erratic flapping further out on the blade. A comparison of hover data to that from a flight in known vortex ring state conditions is shown in Figure 24. [Varnes, 1999]

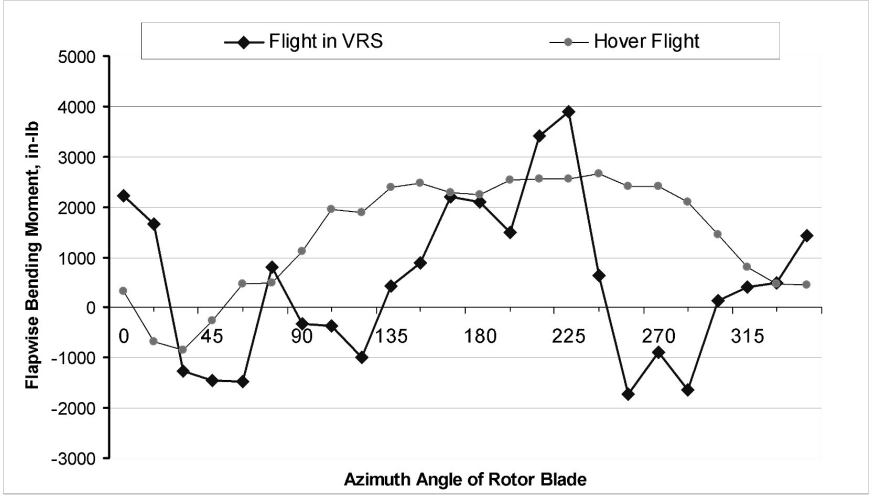

Figure 24. H-34 Flapwise Bending Moment At R/R=0.575.

Analysis of the flapwise bending moment data indicate highly erratic behavior during VRS conditions. Broadly varying flapwise bending moments are evident. Compression of the upper surface of the blade is indicated as positive. Amplitude changes, as well as sharp variations between compression and tension of the upper surface of the blade are shown for the case of VRS. Corresponding large blade deflection is associated with such values. The drastic reversal in compression and tension indicate clearly the many blade vortex encounters expected during VRS. Large discontinuities are produced, since blade and bending moment is the second derivative of blade deflection, the rate of change of the blade slope, or gradient.

3. Harmonic Analysis

Harmonic analysis of section aerodynamic loading was compiled on the five flights listed in Table 2. Considering flapwise and chordwise bending, the following equation was used to compute section aerodynamic loading.

$$l_n(y) = L_0 \sum_{n-1}^{10} [L_n \cos n(y) + M_n \sin n(y)]$$

$L_n(lb/in)$
$M_n(lb/in)$

The section aerodynamic loading, $l_n(y)$ is the integral of chordwise differential pressure per unit span (lb/in) over the blade section length. The integrand was approximated as a sum over ten stations at equal intervals over the full length of the rotor blade. L_n and M_n are harmonic series coefficients of section aerodynamic loading per unit span, lb/in. Resulting harmonic amplitudes are obtained by calculating the square root of the sum of the squares of the coefficients. Figure 25 shows the resulting harmonic amplitudes of section aerodynamic loading, and compares four flights encountering VRS to data taken in a hover.

In the vortex ring state region extremely abrupt changes in airload are a result of blade vortex interaction. Higher harmonic content is prevalent during this period and is the principal contributor to the aircraft vibrations. Study of Figure 25 shows that harmonic analysis of the aerodynamic blade loading may be used to determine the onset of the vortex ring state. There is clearly an indication of the increase in amplitude of higher harmonics as the rotor system encounters VRS. The H-34 has four blades, and we note the corresponding maximum vibration amplitude is seen at 4P, which is four times the operating rotor speed, the blade passage frequency.

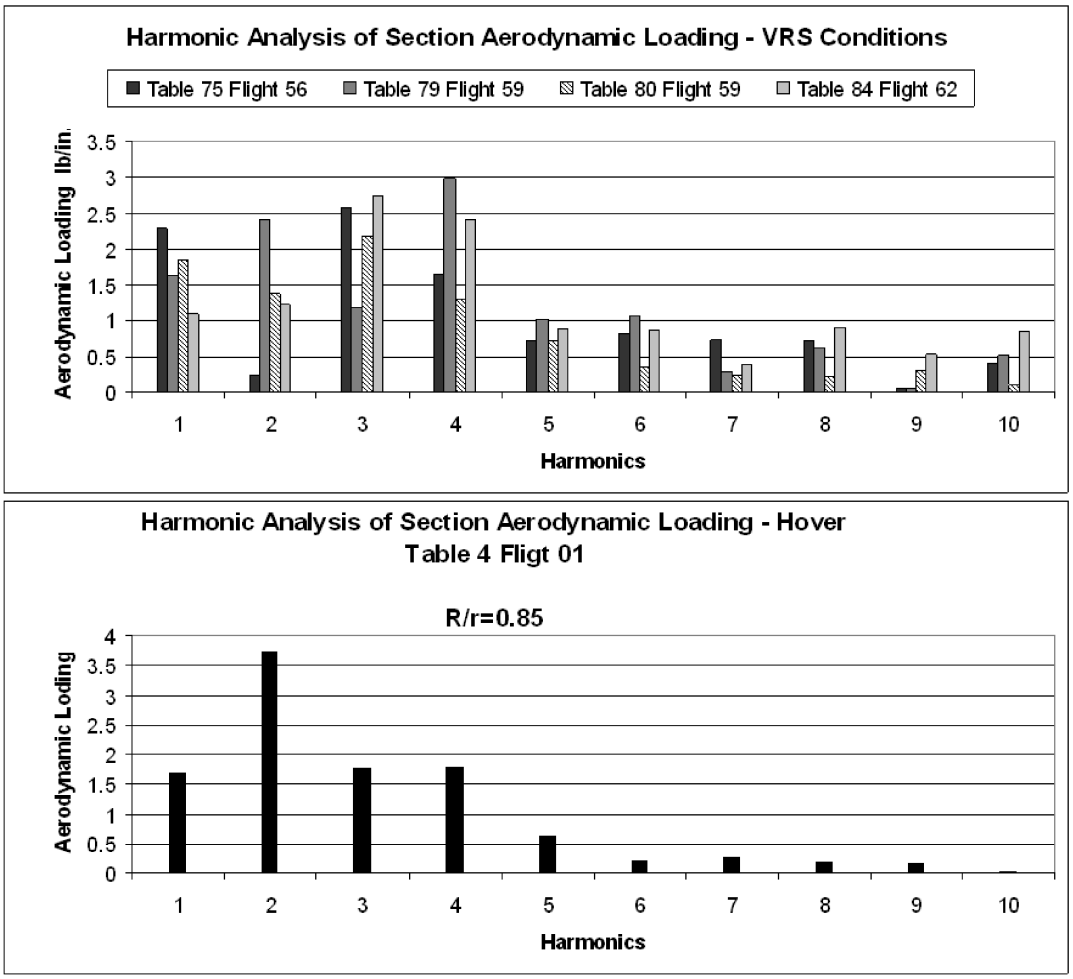

Figure 25. Harmonic Analysis (nP).

Note that Figure 25 shows significant response at all multiples of the rotor operating frequency (1P), whereas Figure 17 does not. This is because Figure 25 shows the section loading spectrum for a single blade, where Figure 17 shows the thrust spectrum for the hub, which filters the single-blade response. Rotor blades are attached at the root to the rotorhead and transmit vibratory responses to the fuselage, or hub, as vibratory shears and moments. Flap and chordwise bending moments produce vibratory shears at the blade root. [Wood, 2000] The rotor head acts like a

filter and only allows frequencies of n/rev (the blade passage frequency) and even multiples of n/rev to pass through.

The amplitude of the aerodynamic loading gives rise to higher harmonics but only 4P and 8P will be transmitted through the rotor system into the airframe. Even multiples of 4P (i.e., 8P, 16P) will begin to appear in the fuselage with increasing amplitude as the onset of increased blade vortex interaction occurs. Lower harmonics of the blade loading are deemed the most prevalent but higher harmonics can be detected.

A comparison of 4P and 8P harmonics to the blade passage frequency (4P) gives a quantifying comparison of the amplitude increases, Table 3. These ratio comparisons can be used to correlate data recorded during the water tunnel investigation. Although, the rotor systems have differing numbers of blades, the ratio of the harmonics show correlation. Compared to hover conditions, there is a significant increase during VRS of the higher harmonic, 8P, when compared to the consistent blade passage frequency. Although, this does not take into account the increase in 4P hub vibrations due to 3P and 5P or the corresponding increase in 8P due to 7P and 9P.

	Hover	**VRS**
4P(averaged)	1.8	2.1
8P(averaged)	0.2	0.7
8P/4P	0.1	**0.3**

Table 3. Maximum Amplitudes and Comparison of Higher Harmonic Magnitudes of Harmonics Listed in Figure 25.

THIS PAGE INTENTIONALLY LEFT BLANK

VI. CONCLUSIONS

A. FLOW VISUALIZATION

The original intent of this investigation was to produce a flow visualization video of a rotor operating in the vortex ring state. The primary motivation was to improve upon the video images captured by the classic Drees and Hendal smoke video from 1951. [Drees, 1951] Filming the flow field on video proved difficult with the limited filming and lighting assets. Although, strobe lights operating at twice the rotational speed of the two-bladed rotor provided superb viewing conditions. With further effort, there is significant potential for capturing valuable images on video.

Images captured using a digital camera were extremely clear. The rotor wake vortices were captured with unexpected clarity. A high speed shutter setting of 1/320 second captured exceptionally clear images of the helical vortex wake. Such images were only seen by the eye when using a strobe light to illuminate the flow field. Fortunately, the high shutter speed camera captured the same images using just flood lighting.

The use of Particle Image Velocimetry should also be considered for use to determine the flow characteristics during VRS. Seeding the flow field with small particles and illuminating them in a single plane would produce interesting results. By tracing the particle motion the velocity of the flow field can be mapped, providing valuable information about VRS flow.

B. VIBRATION ANALYSIS

Data acquired from thrust measurements were analyzed using an FFT analyzer. This revealed surprising correlation between the water tunnel model and actual flight data. An inexpensive water tunnel experiment using a scaled model produced valuable test results. Of primary interest is the thrust-induced vibration power spectrum. These frequency domain data enabled a vibration analysis and identified the presence of increased higher harmonics during VRS flow conditions. The data recorded generated interest to determine if the same increase in harmonics occurred in a full scale aircraft. Analysis of Scheiman data revealed this to be true.

Harmonic analysis of the aerodynamic loading indicates that higher harmonic content becomes prevalent during operation in the vortex ring state and is a contributor to aircraft vibrations. For a two-bladed system, 2P harmonic is present in virtually all regions of flight. Higher harmonics, such as 4P and 6P are typically only present during particular maneuvers encountering blade vortex interaction or if the rotor system is poorly designed.

An accelerometer could provide a warning to the cockpit as higher harmonic amplitudes are detected. High vibrational components to the thrust response may be encountered during various flight conditions but if experienced during a typical steep approach into landing it may be an indicator of the proximity of the VRS boundary. A higher harmonic warning device seems worthy of further investigation.

LIST OF REFERENCES

Brown, R.E., “Rotor Wake Modeling for Flight Dynamic Simulation of Helicopters,” AIAA Journal, Vol. 38, No. 1, 2000.

Brown, R.E., Newman, S.J., Leishman, J.R. and Perry, F.J., “Blade Twist Effects on Rotor Behavior in the Vortex Ring State,” Presented at the European Rotorcraft Forum, Bristol, England, September 2002.

Drees and Hendal, “Aerodynamic Investigation of a Model Helicopter Operating in a Smoke Tunnel,” Video 1951.

Gao, Zheng and Xin, Hong, “An Experimental Investigation on Vortex Ring State Boundary,” First Russian Helicopter Society Annual Forum Proceedings, August 1994.

Gessow, A. and Myers, G., “Aerodynamics of the Helicopter,” Frederick Ungar Publishing, 1952.

Newman, S.J., Brown, R., Perry, F.J., Lewis, S., Orchard, M. and Moda, A., “Comparative Numerical and Experimental Investigation of the Vortex Ring Phenomenon in Rotorcraft,” Proceeding of the 57th Annual Forum of the American Helicopter Society, Washington DC, May 9-11, 2001.

Peters, David, A. and Chen, Shyi-Yuang, “Momentum Theory, Dynamic Inflow, and the Vortex Ring State,” Journal of the American Helicopter Society, July 1982.

Prouty, Raymond W., “Helicopter Performance, Stability, and Control,” PWS Publisher, 1986.

Scheiman, James, NASA Technical Memorandum, X-952, “A Tabulation of Helicopter Rotor-Blade Differential Pressures, Stresses, and Motions as Measured in Flight,” March 1964.

Stewart, W.B. Sc., “Helicopter Behavior in the Vortex Ring Conditions,” A.R.C. R/M-3117, November 1951.

Van Dyke, Milton, “An Album of Fluid Motion,” 1982.

Varnes, David J., “Development of a Helicopter Vortex Ring State Warning System Through a Moving Map Display Computer,” Department of Aeronautics and Astronautics, Naval Postgraduate School, Monterey, California, September 1999.

Wolkovitch, Julian, “Analytical Prediction of Vortex Ring State Boundaries for Helicopters in Steep Descents,” Journal of the American Helicopter Society, July 1972.

Wood, Roberts E., “An Introduction to Helicopter Dynamics,” Department of Aeronautics and Astronautics, Naval Postgraduate School, Monterey, California, September 2000.

Yeates, John E., “Flight Measurements of the Vibrations Experienced by a Tandem Helicopter in Transition, Vortex Ring State, Landing Approach, and Yawed Flight,” National Advisory Committee for Aeronautics, Technical Note 4409, Washington, September 1958.

INITIAL DISTRIBUTION LIST

1. Defense Technical Information Center
   Ft. Belvoir, Virginia

2. Dudley Knox Library
   Naval Postgraduate School
   Monterey, California

3. Marine Corps Representative
   Naval Postgraduate School
   Monterey, California

4. Director, Training and Education, MCCDC, Code C46
   Quantico, Virginia

5. Director, Training and Research, MCCDC, Code C40RC
   Quantico, Virginia

6. Marine Corps Tactical Systems Support Activity (Attn: Operations Officer)
   Camp Pendleton, California

7. Department Chairman, Department of Physics
   Naval Postgraduate School
   Monterey, California

8. Department Chairman, Department of Aeronautics and Astronautics
   Naval Postgraduate School
   Monterey, California

9. Naval Air Systems Command
   PMA-275
   Patuxent River, Maryland